



A comparative study of the steam reforming of phenol towards H₂ production over natural calcite, dolomite and olivine materials

Domna A. Constantinou^a, José Luis G. Fierro^b, Angelos M. Efstathiou^{a,*}

^a Heterogeneous Catalysis Laboratory, Department of Chemistry, University of Cyprus, P.O. Box 20537, CY 1678 Nicosia, Cyprus

^b Instituto de Catálisis y Petroleoquímica, CSIS, C/Marie Curie 2, Cantoblanco, 28049 Madrid, Spain

ARTICLE INFO

Article history:

Received 11 October 2009

Received in revised form 29 December 2009

Accepted 7 January 2010

Available online 14 January 2010

Keywords:

Phenol steam reforming

Hydrogen production

Natural calcite

Dolomite and olivine

XPS

EDX

HRTEM

Transient experiments

CO₂-TPD

H₂-TPR

CO₂-DRIFTS

ABSTRACT

Pre-calcined (air, 850 °C) naturally occurring calcite, dolomite and olivine materials were studied for phenol steam reforming towards H₂ production. The effect of reaction temperature, feed volume flow rate, and hydrogen concentration in the feed stream on phenol conversion, H₂ product concentration and selectivity were investigated. The increase of reaction temperature in the 650–800 °C range led to the increase of phenol conversion and H₂-selectivity for the calcite and dolomite materials, while the opposite behaviour was observed for the olivine material. An increase of phenol conversion was obtained with decreasing Gas Hourly Space Velocity, GHSV in the 40,000–80,000 h^{−1} range for all three natural materials studied. The lower activity (per gram basis) of pre-calcined olivine compared to that of pre-calcined calcite and dolomite at high reaction temperatures (750–800 °C) is suggested to be linked to the increased extent of reducibility of α-Fe₂O₃ and Fe₃O₄, and of Fe_xMg_{1−x}O_y and Ca₂Fe₂O₅ phases likely present (X-ray diffraction measurements) in the pre-calcined olivine into less reactive Fe^{II}O and Fe⁰ under reaction conditions. X-ray photoelectron spectroscopy studies performed over the raw olivine revealed also the presence of Fe^{II}O. Phenol steam reforming reaction followed by transient isothermal oxidation allowed the measurement of “carbonaceous” species that react towards CO and CO₂ and which accumulate during phenol steam reforming, as a function of reaction temperature and time on stream. The lower amount of “carbonaceous” species formed on the surface of calcined olivine under steam reforming of phenol at 650 °C, as well as its higher site reactivity compared to calcite and dolomite are considered likely reasons for the higher activity and H₂-yield exhibited by olivine at 650 °C compared to calcite and dolomite. Comparative studies regarding the CO₂ adsorption characteristics over pre-calcined calcite, dolomite and olivine using *in situ* CO₂-DRIFTS and CO₂-TPDs were conducted. It was found that olivine accommodates significantly lower amounts of CO₂ compared to calcite and dolomite. The effect of hydrogen concentration in the feed stream towards phenol steam reforming activity on dolomite was found to be negative. *In situ* DRIFTS studies using H₂/H₂O/Ar and H₂/H₂O/CO₂/He gas atmospheres suggested that this effect is related to the substantial decrease in the rate of water dissociation to form –OH active species caused by the simultaneous reversible interaction of H₂ with the MgO/CaO surfaces.

© 2010 Elsevier B.V. All rights reserved.

1. Introduction

One of the most important issues associated with the global energy demands is the need for replacing fossil fuels with alternative energy sources benign to the environment [1]. Molecular hydrogen is a clean energy carrier of high calorific value having a strong potential to be utilized in a sustainable future energy economy [2–6]. The full environmental benefit of generating power from hydrogen can be achieved when hydrogen is manufactured using renewable resources, primarily solar, wind and biomass [7,8].

Biomass is abundantly available and CO₂-neutral, and can be considered as one of the future sources for hydrogen production [3,4,7,8].

Among biomass conversion processes, catalytic steam gasification is an attractive process for the production of a hydrogen-rich gas [9–12]. However, one of the major issues in biomass gasification remains the tar formation and its removal from the raw gas product [9,13]. Tar is a complex mixture of condensable hydrocarbons, which includes single-ring to multiple-ring aromatic compounds along with other oxygen-containing hydrocarbons, and contributes in the decrease of the total process efficiency and the increase in cost purification of the product gas [9,13]. Tar formation is highly depended on the operational conditions such as reaction temperature and pressure, type of catalyst, residence time and gasifying

* Corresponding author. Fax: +357 22 892801.

E-mail address: efstath@ucy.ac.cy (A.M. Efstathiou).

agent used [8,13]. It has been reported that the addition of steam can lead to high quality of H₂-rich gas [14,15] due to the formation of fewer refractory tars that are easier to be reformed catalytically [13–17]. This is true especially when wood-biomass gasification is used [17], where phenol was found to be one of the representative constituent molecular species of tar.

The use of naturally occurring dolomite, olivine and calcite materials as catalysts contribute to the hot-gas cleanup required in practical biomass gasification [8,18,19]. These materials are inexpensive, non-toxic, and abundant having good activity at high temperatures [19,20]. In particular, their use in fluidized-bed reactors can be very promising for the conversion of biomass by steam into hydrogen. This process can be more efficient than the practiced gasification method due to the *in situ* integration of the heats of CO₂ absorption and water–gas shift reaction into the gasification/reforming reaction network resulting to an autothermal process with a product gas rich in hydrogen and low in CO content.

Several research groups have investigated tar conversion efficiencies of calcined dolomites (mixture of CaO and MgO) [11,21–28]. Simell et al. [24] investigated the use of dolomites and limestones in calcined and carbonated forms to reform toluene (model tar compound) at 900 °C. They showed that the calcined materials decomposed toluene efficiently but the activity of the carbonated form was practically zero. Taralas et al. [25,26] used calcined dolomite to reform n-heptane and cyclohexane as model tar compounds, where the influence of hydrogen and carbon dioxide on the degree of total conversion was investigated. Aldén et al. [28] investigated the catalytic reforming of naphthalene over dolomite and reported that the presence of H₂O enhanced cracking efficiency.

An attractive group of naturally occurring materials is olivine, a magnesium and iron silicate mineral ((Mg,Fe)₂SiO₄). Rapagná et al. [29] investigated the catalytic activity of calcined olivine and observed that it has a good performance in terms of tar reduction and comparable activity to calcined dolomite. They reported more than 90% reduction in tar content; the tar amounted to 2.4 g/m³ compared to 43 g/m³ obtained with sand. Corella et al. [30] have studied sintered olivines, calcined dolomite and Ni/olivine catalysts for biomass gasification with air in a fluidized bed. They concluded that dolomite was a more effective additive than olivine but the former generated more particulates.

Calcined calcites could be an interesting “*in bed*” material in biomass gasification using fluidized-bed reactors. These materials are the least investigated compared to dolomites and olivines. Delgado et al. [31] have studied calcite, dolomite and magnesite placed downstream of a biomass gasifier, showing that calcite can also be active towards tar removal, especially at high temperatures. Garcia et al. [32] carried out gasification of tars of different origin using CaO obtained by limestone calcination in a fixed-bed reactor. A total conversion to gaseous products was obtained for a steam to tar ratio equal to or larger than 3.5 and at temperatures above 750 °C.

The present work is a continuation of previous work reported from our laboratory [33,34] and is focused on the understanding of the *intrinsic reasons* of the different catalytic activity towards steam reforming of phenol in the 650–800 °C range exhibited by pre-calcined calcite, dolomite and olivine natural materials. Ca- and Mg-containing solids are attractive materials that could play the combined role of catalyst and CO₂-absorbent in steam gasification/reforming processes. The naturally occurring materials studied in this work were identified as the best solids over a series of materials of different geographical origin investigated [17]. It is worth noting that the present naturally occurring olivine material investigated is different from the one used previously by Rapagná et al. [29], a commercially available one (Magnolithe GmbH).

The present work provides important fundamental information on the effects of (a) reaction temperature, (b) feed flow rate, and (c) the presence of H₂ and CO₂ in the feed gas stream on the rate of

phenol steam reforming towards H₂ production over three important naturally occurring materials, namely: calcite, dolomite and olivine. In an effort to develop relationships between important physico-chemical surface properties and catalytic performance parameters related to the present solids, various bulk and surface catalyst characterization techniques such as X-ray Diffraction, BET, EDX chemical analysis, XPS, HRTEM, H₂ temperature-programmed reduction (H₂-TPR), CO₂ temperature-programmed desorption (CO₂-TPD), and *in situ* DRIFTS-CO₂ chemisorption under various gas atmospheres were conducted. The measurement of “carbon” accumulation with reaction time and temperature was also performed and the results obtained were related to the phenol steam reforming activity performance of the three naturally occurring materials investigated.

2. Experimental

2.1. Catalyst characterization

2.1.1. Solid surface texture

The BET method (adsorption of N₂ at 77 K) was carried out in a Micromeritics Gemini III Surface Area and Pore size Analyzer in order to determine the specific surface area (m² g⁻¹), the specific pore volume (cm³ g⁻¹), and the average pore diameter (nm) of given pre-calcined natural calcite, dolomite and olivine materials of different geographical origin [17]. Each measurement was taken after the samples were calcined in air at 850 °C for 2 h and outgassed *in situ* at 200 °C under vacuum ($P \approx 1.3 \times 10^{-3}$) overnight.

2.1.2. X-ray diffraction studies

The crystal structure of the as received (raw) and after calcination in air at 850 °C for 2 h natural materials was checked by X-Ray diffraction (XRD) (Shimadzu 6000 diffractometer, Cu-K_α radiation ($\lambda = 1.5418 \text{ \AA}$)). The mean primary crystallite size (d_c , nm) of the calcined natural calcite, dolomite and olivine materials was determined using the Scherrer equation [35]. Each sample was crushed and sieved to lower than 200 mesh size before measurements were performed. The diffractograms were taken in the 10–100° 2 θ range with a step of 2°/min.

2.1.3. HRTEM and EDX spectroscopy studies

The morphology of the natural materials was examined by High Resolution Transmission Electron Microscopy (HRTEM) using a JEOL 2100F transmission electron microscope with a field emission gun (FEG) and a point resolution of 0.19 nm. The elemental chemical analysis of the natural calcite, dolomite and olivine samples was performed using the EDXS thin-window energy dispersive X-ray spectrometer (INCA x-sight, Oxford Instrument) coupled with TEM microscope. The wt% composition of each sample was determined by the aid of provided instrument's software and appropriate calibration procedures. The specimens were prepared by ultrasonically dispersing the powder sample in iso-octane and placing a droplet of the suspension on a copper grid covered with a carbon film.

2.1.4. X-ray photoelectron spectroscopy studies

X-Ray photoelectron spectroscopy (XPS) studies were conducted on a VG Escalab 200R electron spectrometer equipped with a hemi-spherical electron analyser and an Al-K_α ($h\nu = 1486.6 \text{ eV}$) X-ray source. The powder samples were pressed in an 8-mm diameter copper trough and fixed on the XYZ manipulator. The base pressure in the analysis chamber was maintained below 4×10^{-9} mbar during data acquisition. The pass energy of the analyser was set at 50 eV for which the resolution measured by the full-width at half maximum (FWHM) of the Au 4f_{7/2} core level was

1.7 eV. The binding energies were referenced to the C1s peak at 284.9 eV (adventitious carbon). Data processing was performed with the XPS peak program, and the spectra were deconvoluted with a least squares fitting routine after subtracting a Shirley background and using Gaussian/Lorentzian (90/10) product function. Atomic composition (atom%) was calculated using peak areas normalized on the basis of sensitivity factors [36]. The estimated error of the quantitative surface composition performed based on duplicate and/or triplicate measurements was within $\pm 8\%$.

2.1.5. H_2 temperature-programmed reduction studies

H_2 temperature-programmed reduction (H_2 -TPR) experiments were conducted in a specially designed gas flow-system previously described [37]. These experiments were performed over the as received and after 2 h pre-calcined olivine material in 20% O_2 /He at 850 °C ($W = 0.5$ g, 30 N mL/min). The temperature was first increased to 850 °C in He flow for 30 min in order to remove any moisture present. After this pre-treatment step the feed was changed to He for 15 min and the sample was cooled to room temperature. A 2 vol% H_2 /He gas mixture was then passed over the catalyst and the temperature was increased to 850 °C at the rate of 30 °C/min. The exit gas from the reactor was monitored by *on line* mass spectrometer (Omnistar, 1–300 amu, Baltzers). The mass numbers (m/z) 2, 18, 32 were used for H_2 , H_2O and O_2 , respectively. Based on a material balance, the rate of hydrogen consumption ($\mu\text{mol } H_2/\text{g s}$) versus temperature was estimated.

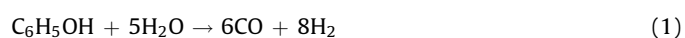
2.1.6. CO_2 temperature-programmed desorption of carbon dioxide (CO_2 -TPD)

Temperature-programmed desorption of CO_2 experiments were conducted in a specially designed gas flow-system described elsewhere [37]. The solid samples ($W = 0.5$ g) of the as received natural calcite, dolomite and olivine were first calcined in 20% O_2 /He at 850 °C for 2 h, purged in He and then cooled quickly to room temperature. The feed was subsequently switched to 2% CO_2 /He (30 N mL/min) gas mixture for 30 min, and then to He for approximately 15 min until no signal of CO_2 was detected in the mass spectrometer. The temperature of the solid was then increased linearly from room temperature to 800 °C ($\beta = 30$ °C/min) in order to carry out a TPD experiment. Calibration of the CO_2 signal ($m/z = 44$) of the mass spectrometer was made based on a 1 vol% CO_2 /He calibration gas mixture.

2.2. Catalytic activity studies

The experimental set-up used for evaluating the catalytic performance of the natural materials towards steam reforming of phenol was described in detail elsewhere [38]. The amount of solid loaded in the fixed-bed micro-reactor was 0.3 g, and the total flow rate used was 200 N mL/min. The reaction feed gas mixture consisted of 0.6% C_6H_5OH /40% H_2O /He, simulating the phenol and water concentrations encountered at the inlet (bottom) of the fluidized-bed used in wood-biomass steam gasification process [17]. Initially, the catalyst sample was calcined in 20% O_2 /He gas mixture at 850 °C for 2 h. All catalytic tests were conducted at 1 bar total pressure in the 650–800 °C range. Following reaction at a given temperature, the catalyst was then treated in 20% O_2 /He at 850 °C for 2 h before proceeding to the next reaction temperature.

The steam reforming of phenol over the calcined calcite, dolomite and olivine can be described by the following reaction network [17,38–42]:



Eq. (3) refers to the calcined calcite and dolomite. In the case of calcined dolomite, $MgCO_3$ was always converted to MgO under the conditions used, while in the case of olivine the main solid phases present could also adsorb CO_2 [24]. The most important parameters for catalyst evaluation in the present work are considered the conversion of phenol, X_p (%), and the selectivity of reaction towards hydrogen, S_{H_2} (%) based on the following relationships [34]:

$$X_p(\%) = \frac{(F_{CO}^{out} + F_{CO_2}^{out})}{6F_p^{in}} \times 100 \quad (4)$$

$$S_{H_2}(\%) = \frac{y_{H_2}^{out}}{y_{H_2}^{max}} \times 100 \quad (5)$$

where, F_i^{out} and y_i^{out} are the molar flow rate and mole fraction of gaseous species i , respectively, in the dry-product gas stream (after removing the water). It is important to note that only very small concentrations of benzene and methane were detected in the dry-product gas stream, and these are not included in Eq. (4). Also, only minor cumulative amounts of benzene were measured in the condensate (water, phenol, benzene) [38]. These results provide the estimate that carbon balance is within 10% for the present catalytic measurements. The effect of total feed volumetric flow rate, 150–300 N mL/min equivalent to 40,000–80,000 h^{-1} GHSV, and of H_2 feed concentration (0–30 vol%) on phenol conversion, hydrogen selectivity, and CO/CO_2 product ratio were also investigated.

The feed gas reaction stream was pre-heated to 250 °C before entering the catalytic reactor [38]. A heating zone of 10 cm in length from the inlet of the reactor to the top of the catalyst bed assured heating of gas at the desired set temperature (top layer of catalyst bed).

2.3. Carbon deposition

The amount of “carbonaceous” intermediate species accumulated on the surface of pre-calcined natural materials after phenol steam reforming at a given reaction temperature and time on stream was measured following an isothermal oxygen titration. Following reaction of 0.6% C_6H_5OH /40% H_2O /He at 650 or 800 °C for 5 and 20 min, the feed was changed to He until the CO ($m/z = 28$) and CO_2 ($m/z = 44$) mass spectrometer signals reached their respective baseline value. The gas flow was then switched to 20% O_2 /He gas mixture and the signals of CO and CO_2 were continuously recorded by *on line* mass spectrometer. The amount of surface “carbon” deposits ($\mu\text{mol C/g catalyst}$) was calculated based on the CO and CO_2 transient response curves calibrated against standard mixtures and using the appropriate carbon mass balance for a flow-reactor.

2.4. *In situ* DRIFTS studies

A Perkin-Elmer Spectrum GX II FTIR spectrometer equipped with a high-temperature/high pressure controllable DRIFTS cell (Harrick, Praying Mantis) was used for performing *in situ* DRIFTS- CO_2 chemisorption studies. About 35 mg of the natural calcite or dolomite or olivine material (pre-calcined *ex situ* at 850 °C in air for 2 h) in a fine powder form was placed firmly into the ceramic cup of the DRIFTS cell. Before any spectrum was recorded the sample was pre-treated *in situ* in 20% O_2 /Ar at 600 °C for 2 h. Chemisorption was performed using both a 2% CO_2 /He gas mixture (100 N mL/min) at 25 and 600 °C, and a 2% CO_2 /40% H_2O /30% or 50% H_2 /He gas mixture (100 N mL/min) at 600 °C. Temperature-programmed desorption-DRIFTS spectra were recorded after 30-min of 2% CO_2 /He adsorption at 25 °C followed by a purge of DRIFTS cell in Ar-flow for 15 min, and a temperature increase to 600 °C. DRIFTS spectra were recorded every 100 °C.

In addition, chemisorption experiments were performed on the pre-calcined dolomite material using a 40% $\text{H}_2\text{O}/30\%$ or 50% H_2/Ar gas mixture (100 N mL/min) at 600 °C. It is important to note here that blank experiments using a 30% or 50% H_2/Ar (100 N mL/min) gas mixture were performed in order to investigate any changes in absorptivity and reflectivity of the solid sample due to likely partial reduction of CaO and/or MgO by hydrogen at 600 °C, which would lead to false interpretation of results. The spectrum difference (absorption mode) obtained after subtracting the spectrum of the solid recorded under Ar flow at 600 °C and that under 30% H_2/Ar or 50% H_2/Ar flow at 600 °C provided zero absorption. This result clearly demonstrates that the presence of hydrogen in the gas treatment of the solid *had no observable effect* on the surface/subsurface structure (e.g. solid reduction) of CaO and MgO. Another blank experiment performed was to check any differences in the DRIFTS spectra of the solid recorded in the 2500–1100 cm^{-1} range under Ar or 40% $\text{H}_2\text{O}/\text{Ar}$ at 600 °C following calcination of the sample as described previously. The result was that no differences were observed.

Regarding the isothermal behaviour of the DRIFTS cell used in the present work, it is noted that no more than 5 °C difference in the temperature of the solid bed (about 2 mm depth) under He or Ar inert gas flow is expected according to the manufacturer (Harrick Scientific). Furthermore, catalytic experiments using the same amount of catalyst as that used in the DRIFTS cell (35 mg) and under the same space velocity conducted in a typical micro-reactor cell (7 mm i.d.) showed no more than 15% difference in catalyst's activity. This result suggests that channelling effects within the catalytic bed of the DRIFTS cell must be considered small.

It is important to note that each DRIFTS spectrum presented here corresponds only to the spectrum of the adsorbed phase since subtraction of the spectrum due to the solid itself taken in Ar or H_2/Ar or $\text{H}_2\text{O}/\text{Ar}$ flow at the desired temperature was performed. DRIFTS spectra when necessary were smoothed to remove high frequency noise and further analyzed using the software Spectrum for Windows. Deconvolution and curve fitting procedures of the DRIFTS spectra were performed according to reported guidelines [43] and using Gaussian peak line shapes [44]. In all DRIFTS spectra recorded signal averaging was set to 50 scans per spectrum at a 2 cm^{-1} spectra resolution in the 4000–400 cm^{-1} range.

3. Results and discussion

3.1. Catalyst characterization

3.1.1. Catalyst texture

The specific surface area (BET, $\text{m}^2 \text{g}^{-1}$), the specific pore volume (cm^3/g), and the average pore diameter (nm) of the natural calcined calcite, dolomite and olivine materials are given in Table 1. It is

Table 1
Textural properties and mean primary crystal size of naturally occurring calcite, dolomite and olivine materials, after calcination in air at 850 °C for 2 h.

Natural material	Physical properties	After calcination (850 °C)
Calcite	BET ($\text{m}^2 \text{g}^{-1}$)	8.0
	Pore volume (cm^3/g)	0.019
	Average pore diameter (nm)	7.5
	Mean primary crystal size (nm)	51.3
Dolomite	BET ($\text{m}^2 \text{g}^{-1}$)	12.6
	Pore volume (cm^3/g)	0.035
	Average pore diameter (nm)	9.0
	Mean primary crystal size (nm)	39.9
Olivine	BET ($\text{m}^2 \text{g}^{-1}$)	0.9
	Pore volume (cm^3/g)	0.001
	Average pore diameter (nm)	4.3
	Mean primary crystal size (nm)	26.6

observed that the calcined dolomite exhibits the highest specific surface area, pore volume, and mean pore diameter compared to calcite and olivine materials in good agreement to what reported [45,46]. On the other hand, calcined olivine was found to have a very low surface area (0.9 m^2/g) and pore volume (0.001 cm^3/g). A pore diameter of 4.3 nm close to that reported (3–4 nm) [47,48] was found.

3.1.2. XRD studies

Fig. 1a–c present X-ray diffractograms of the natural calcite, dolomite and olivine materials as received and after calcination at 850 °C (see Section 2.1.2). The raw calcite material exhibits characteristic 2θ -diffraction peaks (Fig. 1a) consistent to the cubic structure of CaCO_3 (JCPDS file 86-174), while after calcination new

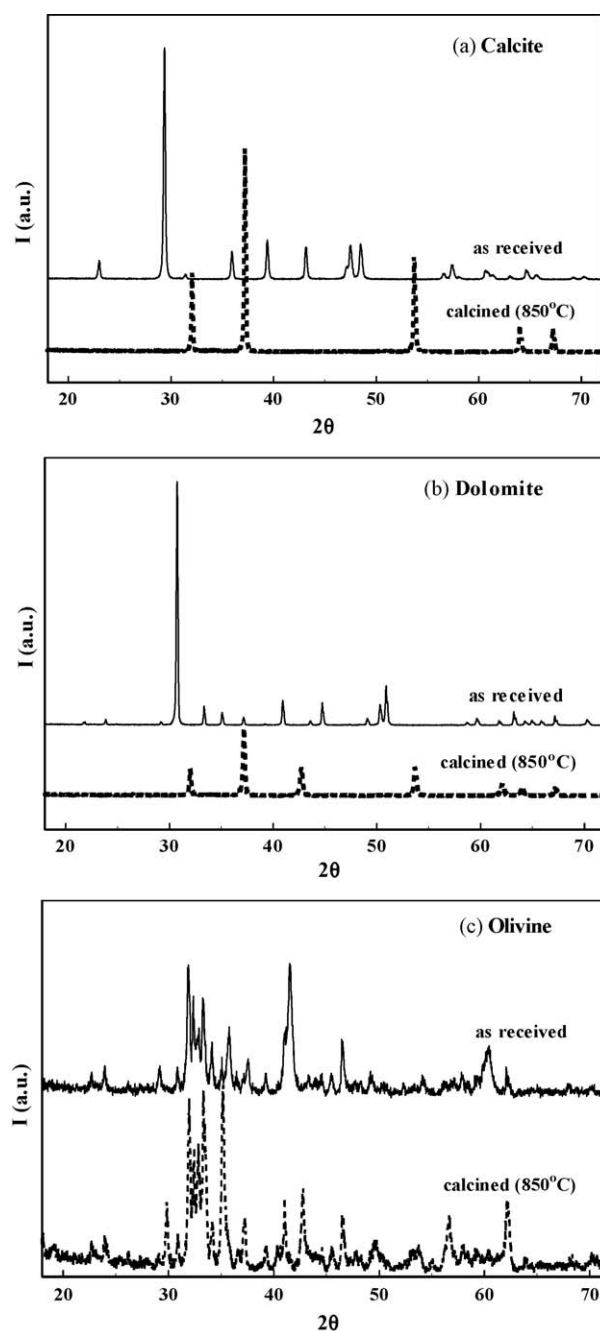


Fig. 1. X-ray diffraction patterns of naturally occurring calcite (a), dolomite (b), and olivine (c) as received (raw) and after calcination in air at 850 °C for 2 h.

diffraction peaks corresponding to the cubic structure of crystalline CaO (JCPDS file 77-2376) were detected as previously discussed [33,34]. Fig. 1b indicates that the characteristic 2 θ -diffraction peaks observed (30.76, 50.9, and 41) correspond to the CaMg(CO₃)₂ structure (JCPDS file 36-0426) [49]. These peaks were absent after calcination, while new diffraction peaks attributed to the cubic structure of MgO (42.74 and 62.16) (JCPDS file 4-0829) and CaO (32.04, 37.20 and 53.72) (JCPDS file 77-2376) were seen [49].

Fig. 1c shows a more complex diffractogram with main 2 θ -diffraction peaks attributed to the presence of CaFeSiO₄ kirschsteinite (30.88, 31.94, 32.38, 33.32, 35.78 and 49.2) [50] and Mg₂SiO₄ forsterite (23.98, 32.84, 37.62, and 54.18) (JCPDS file 34-0189) phases which belong to the olivine group of materials having an orthorhombic structure [49–52]. In addition, diffraction peaks of FeO (35.08, 35.78, 41.6, 60.46) (JCPDS file 46-1312) were detected in the raw olivine material [53,54]. The fact that FeO (wüstite) is present in the raw olivine was also confirmed by X-ray photoelectron spectroscopy studies (see Section 3.1.4). The results of Fig. 1c lead to the conclusion that the solid studied is a Ca-containing natural olivine [55] in agreement with the elemental composition (wt%) and atomic surface concentration (atom%) derived after using energy dispersive X-ray and X-ray photoelectron spectroscopy techniques, respectively (see Tables 2 and 4).

After calcination of the raw naturally occurring olivine material at 850 °C, characteristic intense 2 θ -diffraction peaks corresponding to α -Fe₂O₃ hematite (35.24, 41.04, 49.76, 53.8; JCPDS file 33-0664) and Fe₃O₄ (29.84, 42.8, 56.72, 62.2; JCPDS file 65-3107) crystal phases had been observed. The latter observation has also been reported by Devi et al. [48] who studied the catalytic activity of an olivine material towards steam reforming of naphthalene (model biomass-derived tar compound). Liu et al. [56] reported X-ray diffraction results regarding Fe_{1-x}Mg_xO_y and Fe₃O₄ oxide films. It was observed that by introducing Mg²⁺ into the Fe₃O₄ spinel structure the intensities of the main diffraction peaks of the latter solid crystal structure decreased, where at $x > 0.5$ these had been disappeared. Based on the results of Fig. 1c for the calcined olivine material and what mentioned above, a partial formation of a mixed Fe_{1-x}Mg_xO_y spinel structure might have been occurred. Sharma et al. [57] and Hirabayashi et al. [58] reported powder X-ray diffraction data of Ca₂Fe₂O₅ solid (brownmillerite structure). The most intense diffraction peaks were recorded in the 32–35° 2 θ range. Therefore, it is not excluded that this crystal phase might have been formed after reaction of some free CaO (present in the naturally occurring olivine) with α -Fe₂O₃ at 850 °C.

The mean primary crystal size of the present calcined naturally occurring materials was estimated using the Scherrer's equation (Table 1). As seen in Table 1, the primary mean crystal size of calcite was significantly larger than that of olivine and to a lesser degree of dolomite.

Table 2

Elemental chemical analysis (wt%) of the naturally occurring calcite, dolomite and olivine solids obtained by EDXS.

Element	Calcite	Dolomite	Olivine
Ca	48.3	28.5	32.8
O	31.6	44.3	18.7
C	17.3	9.6	9.3
Mg	0.4	16.9	10.4
Si	0.09	0.7	6.5
Sn	0.8	–	–
Sb	1.5	–	–
Fe	–	–	20.2
Mn	–	–	0.7
Al	–	–	1.4

3.1.3. EDX and HRTEM studies

Table 2 presents the elemental composition (wt%) of the raw natural calcite, dolomite and olivine materials as determined by EDX analysis. It is observed that the calcite contains small amounts of metal impurities (<0.8 wt%) with slightly larger amounts of Sb (1.5 wt%). These results agree to those obtained by XRD measurements (Fig. 1a), where only crystalline CaCO₃ was present in the raw calcite which decomposed to CaO after calcination [34]. For the dolomite material the only metal impurity detected was Si (0.7 wt%). These results are also in harmony with the XRD studies (Fig. 1b), where besides CaMg(CO₃)₂ no other metal carbonate phases could be seen in the case of the raw dolomite material. The olivine material was found to contain small amounts of Mn (0.7 wt%) and Al (1.4 wt%), and high amounts of Ca (32.8 wt%), Fe (20.2 wt%), Mg (10.4 wt%) and Si (6.5 wt%), confirming the X-ray diffraction peaks identified (see Fig. 1c).

Figs. 2 and 3 show HRTEM images obtained on the raw natural dolomite and olivine materials, respectively. In particular, Fig. 2a and b show HRTEM micrographs for the raw natural dolomite at a low (100 nm scale unit) and high magnification (5 nm scale unit), respectively. Similar HRTEM images are shown in Fig. 3a (100 nm

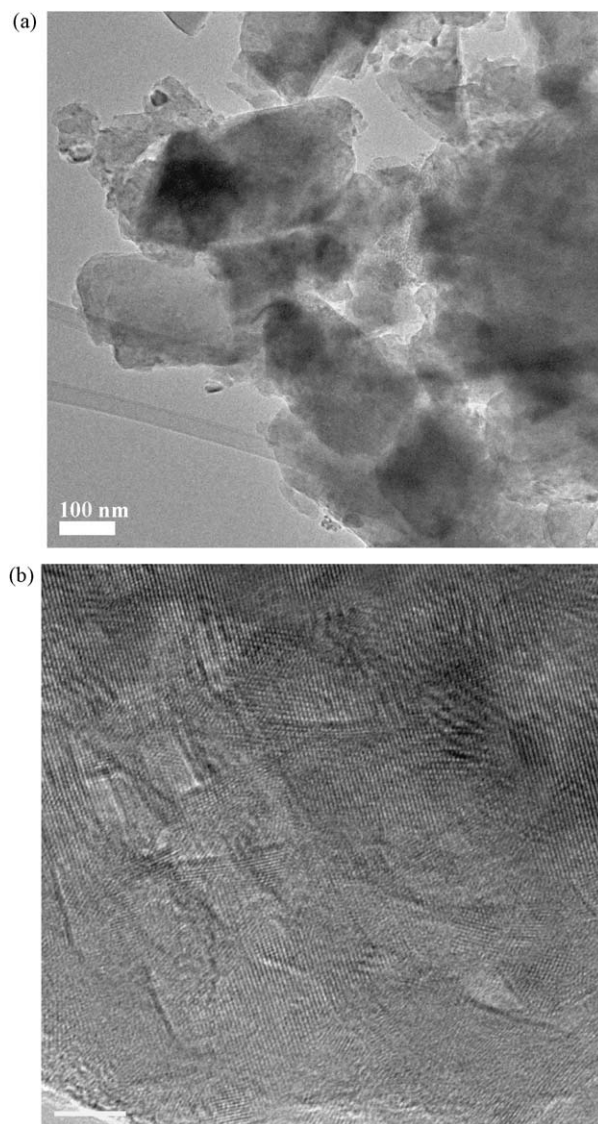


Fig. 2. HRTEM images of the raw naturally occurring dolomite at different magnifications. Scale unit in each photo is: (a) 100 nm; (b) 5 nm.

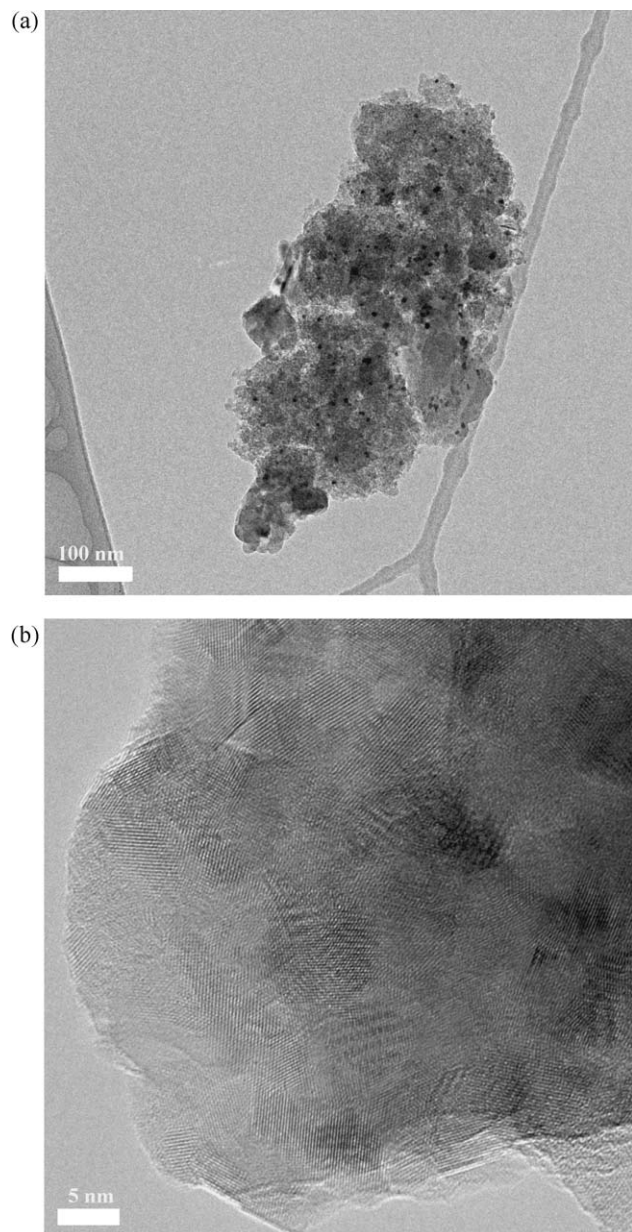


Fig. 3. HRTEM images of the raw naturally occurring olivine at different magnifications. Scale unit in each photo is: (a) 100 nm; (b) 5 nm.

scale unit) and 3b (5 nm scale unit) for olivine. HRTEM photographs obtained for the raw naturally occurring calcite were reported previously [34].

At the low magnification (Fig. 2a, 100 nm) dolomite sample seems to contain particles formed by aggregates of smaller particles having irregular shape and random orientation, while at the high magnification (Fig. 2b, 5 nm) an excellent quality of micrograph was obtained showing that dolomite sample is built up of crystalline micro-domains of carbonate phases (Ca,Mg) ran-

domly oriented. In addition, the HRTEM micrograph allows to measuring the interspacing between the atomic layers of dolomite. This is found to be approximately 0.3 nm in good agreement with the reported value of 0.288 nm [59]. In the case of olivine, the low magnification HRTEM micrograph (Fig. 3a) obtained showed rather large iron oxides particles dispersed in the sample matrix. Based on the XRD (Fig. 1c) and XPS (see Section 3.1.4) results, these iron oxides particles present in the raw material belong to FeO (wüstite). Moreover, the high magnification micrograph obtained for the raw olivine (Fig. 3b) revealed regions in the sample where interspacing of atomic layers was possible to be seen with an approximate value of 0.29 nm.

3.1.4. X-ray photoelectron spectroscopy studies

Table 3 reports binding energies of the core electrons of Ca, C, O, Mg, Fe and Si measured on the natural calcite, dolomite and olivine materials studied. In the case of natural calcite, characteristic photoemission peaks including Ca 2p_{3/2} (347.1 eV), Ca 2p_{1/2} (350.4 eV), O 1s (531.6 eV), and C 1s (289.7 eV) were identified. A surface atom ratio of CO₃²⁻/Ca = 1.14 was estimated in agreement with the bulk stoichiometric ratio of CaCO₃. The latter peaks fit also well with the expected reported values for a naturally occurring calcite material [60–62]. Additional photoelectron peaks at 50.1 and 102.8 eV were observed for the dolomite material assigned to Mg 2p and Si 2p, respectively. The dolomite surface was also found to be carbonated with a CO₃²⁻/Ca ratio being almost two equivalent surface monolayers. In addition, the CO₃²⁻/Ca ratio estimated in the case of olivine was approximately one equivalent surface monolayer. It is interesting to mention that in the case of raw dolomite the binding energy of Ca 2p_{3/2} is slightly lower (346.7 eV) compared to reported values [63] probably due to the formation of some calcium silicate. The latter was also observed in the olivine material.

The XPS studies conducted over the raw olivine material revealed that small fraction (~30%) of calcium is in the form of CaO, while the rest is a mixture of calcium carbonates and silicates. The binding energies of Fe 2p_{3/2} and Fe 2p_{1/2} recorded at 710.8 and 725.1 eV, respectively, had also being detected for the raw natural olivine as seen in Fig. 4. This spectrum is characteristic for air-exposed FeO powder [64]. Based on the reported results, a satellite peak which indicates the presence of Fe^{III} species is detected at approximately 8.0 eV above the parent Fe 2p_{3/2} peak (718.8 eV) [64,65]. This is due to the covering of FeO with a layer of α-Fe₂O₃. The latter is known to take place in the case of air-exposed powders of FeO and Fe₃O₄ because both solids are thermodynamically unstable in air and tend to be covered with a layer of α-Fe₂O₃ [64].

Table 4 reports the surface atom% composition of the raw natural calcite, dolomite and olivine materials. In the case of calcite it is observed that metal impurity levels were significantly low (<0.4 atom%) in agreement with the XRD measurements (Fig. 1a), where besides CaO no other metal oxide phase due to these metal impurities could be detected after calcination [33,34]. Similar results were also found for dolomite; only low levels of Si (0.7 atom%) were found on the surface of CaMg(CO₃)₂ material. The surface elemental composition of the raw olivine material confirmed the observations made in the XRD studies (Fig. 1c)

Table 3

Characteristic binding energies (eV) of core electrons in the raw naturally occurring calcite, dolomite, and olivine solids.

Sample	Ca 2p _{3/2}	Ca 2p _{1/2}	O 1s	C 1s	Mg 2p	Fe 2p _{3/2}	Fe 2p _{1/2}	Si 2p
Calcite	347.1	350.4	531.6	289.7	–	–	–	–
Dolomite	346.7	350.3	531.5	289.6	50.1	–	–	102.8
Olivine	346.6	350.3	531.8	289.5	50.2	710.8	725.1	102.9

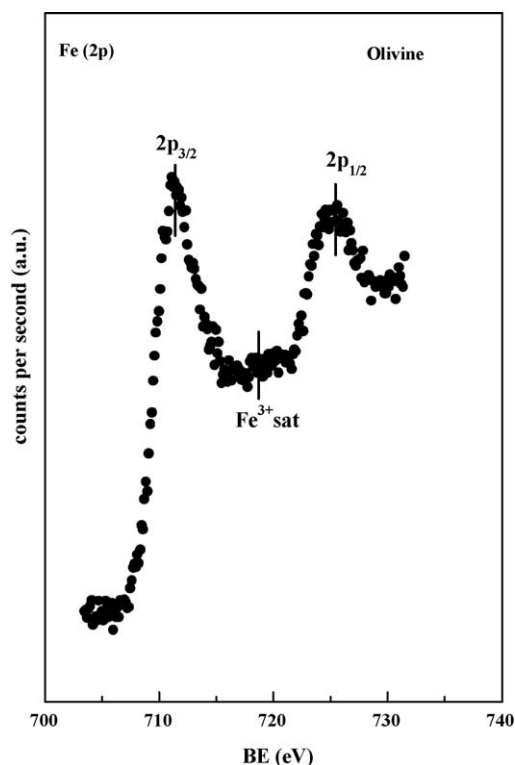


Fig. 4. X-Ray photoelectron spectra of Fe (2p) core level obtained on the raw naturally occurring olivine.

that the solid investigated is a Ca-rich naturally occurring olivine material.

3.1.5. H_2 -TPR studies

It is known that the catalytic activity of Fe-containing materials towards steam reforming depends to a great extent on the oxidation state of Fe (Fe^{2+} or Fe^{3+}) [48,51,52]. The naturally occurring olivine investigated in the present work contains a high amount of surface and bulk iron (Tables 2 and 4). Hence, it is important to understand the behaviour of this material in a reducing environment since H_2 is a product gas of the phenol steam reforming reaction. The hydrogen temperature-programmed reduction profiles of the raw and after calcination (850 °C) natural olivine materials are shown in Fig. 5. The raw olivine material consumed nearly twelve times lower amount of hydrogen than the pre-calcined at 850 °C olivine. Reduction of FeO (wüstite) was reported to take place in the 150–350 °C range (the case of raw material) and it is independent of the kind of gas atmosphere used, e.g. inert He or hydrogen gas [54]. Moreover, it is noted that reduction of FeO may take place in one-step: $Fe^{II}O \rightarrow Fe^0$, or in a two-step pathway: $3Fe_2O_3 \rightarrow 2Fe_3O_4 \rightarrow 6Fe$ up to 570 °C, or in a three-step pathway: $3Fe_2O_3 \rightarrow 2Fe_3O_4 \rightarrow 6FeO \rightarrow 6Fe$ up to 880 °C [54]. The latter pathway was postulated when the temperature of

Table 4

Surface composition (atom %) of the naturally occurring calcite, dolomite and olivine solids measured by X-ray photoelectron spectroscopy.

Element	Calcite	Dolomite	Olivine
Ca	16.6	9.7	14.1
O	50.9	60.8	63.0
C	32	20.6	10.8
Mg	0.4	8.2	1.2
Si	0.04	0.7	6.2
Sn	0.03	–	–
Sb	0.03	–	–
Fe	–	–	4.7

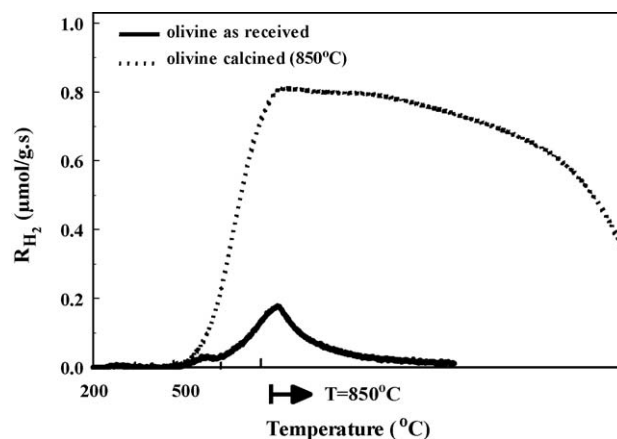


Fig. 5. Hydrogen temperature-programmed reduction (H_2 -TPR) traces in terms of rate of hydrogen consumption ($\mu\text{mol } H_2/(\text{g s})$) versus temperature obtained over the raw and calcined olivine. $F_{H_2/He} = 30 \text{ N mL/min}$; $\beta = 30 \text{ }^\circ\text{C/min}$; $W = 0.5 \text{ g}$.

reduction exceeds 570 °C [54]. A more symmetrical shape in the H_2 -TPR peak is a characteristic feature of reduction of wüstite (FeO) [54] as observed in the present raw olivine material (Fig. 5, olivine as received). The H_2 -TPR trace for the olivine calcined at 850 °C shows a totally different transient isothermal (850 °C) reduction behaviour compared to that obtained in the case of the as received olivine material. A very broad isothermal reduction profile corresponding to a significantly larger amount of hydrogen consumed is observed in the case of calcined as opposed to the as received (not calcined) olivine material.

As discussed in the previous Section 3.1.2, calcination of the as received olivine ($CaFeSiO_4$, Mg_2SiO_4 and FeO) results in the conversion of FeO to $\alpha\text{-Fe}_2O_3$ and Fe_3O_4 . The fact that the amount of iron able to be reduced was largely increased after calcination of the raw olivine material at 850 °C (compare H_2 -TPR traces in Fig. 5) strongly suggests that the iron present in the $CaFeSiO_4$ phase was partly converted into iron oxides, as it can also be suggested by the increase in the intensity of 35.8° 2θ X-ray diffraction peak shown in Fig. 1c. Furthermore, the shape of the transient isothermal (850 °C) reduction curve in the case of calcined olivine suggests a multiple reduction process of iron oxides as previously discussed.

3.1.6. CO_2 chemisorption at 25 °C followed by TPD

Fig. 6 presents CO_2 temperature-programmed desorption response curves obtained on the pre-calcined natural calcite,

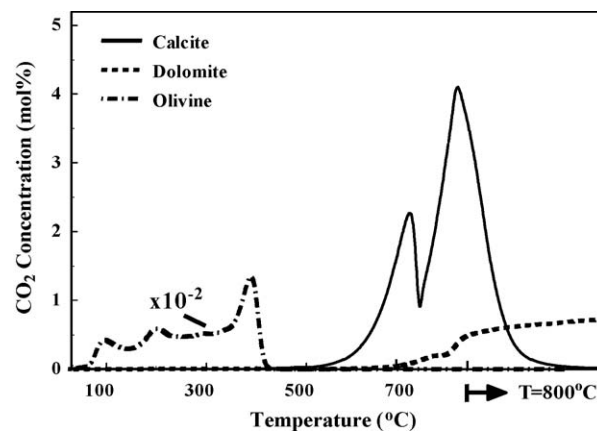


Fig. 6. CO_2 temperature-programmed desorption (TPD) response curves obtained under He flow over the naturally occurring calcite, dolomite and olivine solids. Adsorption conditions: 2 vol% CO_2/He , 25 °C, 30 min. Desorption conditions: $Q_{He} = 30 \text{ N mL/min}$, $\beta = 30 \text{ }^\circ\text{C/min}$.

Table 5

Peak maximum desorption temperatures (T_{\max}) and amounts of adsorbed CO_2 ($\mu\text{mol/g}_{\text{cat}}$) estimated from CO_2 -TPD experiments over naturally occurring calcite, dolomite and olivine solids.

Natural material	$T_{\max}^{(1)}$ (°C)	$T_{\max}^{(2)}$ (°C)	$T_{\max}^{(3)}$ (°C)	$T_{\max}^{(4)}$ (°C)	$\mu\text{mol/g}$
Calcite	711	800	–	–	481
Dolomite	768	800	–	–	156.5
Olivine	98	201	297	390	1.53

dolomite and olivine solids following chemisorption of 2% CO_2 /He at room temperature. In the case of calcite material, two distinct CO_2 desorption peaks were observed with peak maxima at 711 and 800 °C (Table 5) and shoulders at the rising part of the low-T peak and at the falling part of the high-T peak, respectively, in agreement with reported works [33,34]. The high CO_2 desorption temperature indicates the high strength of basic sites of CaO surface, in harmony with the literature [66,67]. The CO_2 -TPD results (Fig. 6) imply that at least two adsorbed states of CO_2 are formed on the surface of CaO in accordance to *in situ* DRIFTS studies [33,34].

The CO_2 -TPD response curve of natural pre-calcined dolomite consists of two broad peaks. The second peak was formed isothermally at 800 °C. The CO_2 desorption profile obtained over natural dolomite depends mainly on the presence of CaO and MgO formed after calcination of dolomite (Fig. 1b). It is known that the basic MgO sites are weaker than those of CaO [66] suggesting that CO_2 adsorbed on MgO should desorb at lower temperatures compared to the CO_2 adsorbed on CaO [53,66]. Based on reported results [24,66,68] the desorption of CO_2 on MgO is completed up to 600 °C. For the present dolomite, only a very small amount of CO_2 was desorbed in the 160–515 °C range (not shown in Fig. 6 due to the scale unit used), very likely corresponding to adsorption of CO_2 on MgO. Thus, it can be suggested that for the present dolomite CO_2 is mainly adsorbed on CaO. In spite of the larger amount per gram basis of CaO than of MgO present in the dolomite (Table 2), the number of adsorption sites per gram basis related to CaO or MgO will depend also on the surface area of each phase.

Four relatively well-resolved carbon dioxide desorption peaks (peak maxima at 98, 201, 297 and 390 °C) were obtained for the pre-calcined natural olivine indicating the presence of different in strength surface basic sites. This result is consistent with the surface elemental analysis obtained (Table 4), where Ca, Mg, and Fe are present, thus, providing different M-O-M' chemical environment and surface basic strength distribution. In addition, it is concluded from the results of Fig. 6 that the basic sites of natural olivine are weaker (lower desorption temperatures) compared to the surface sites of calcite and dolomite, in harmony with other published works [63].

The quantity ($\mu\text{mol/g}$) of basic sites was obtained after integrating the respective CO_2 desorption curves and accounting for the time needed at 800 °C in He flow until no desorption of CO_2 had been detected (Fig. 6). The estimated values are reported in Table 5. It is seen that the amount of CO_2 desorbed from the surface of CaO (calcined calcite) is nearly three times larger than the amount of CO_2 desorbed from the calcined dolomite, and significantly larger than that obtained from the calcined olivine.

3.2. Catalytic performance of pre-calcined natural calcite, dolomite and olivine materials

3.2.1. Effect of reaction temperature

Fig. 7a and b present results of the effect of reaction temperature on phenol conversion, X_p (%), and hydrogen selectivity, S_{H_2} (%), respectively, following the 0.6% $\text{C}_6\text{H}_5\text{OH}/40\%\text{H}_2\text{O}/\text{He}$ reaction over the natural pre-calcined calcite, dolomite and olivine materials. Both phenol conversion and hydrogen selectivity were

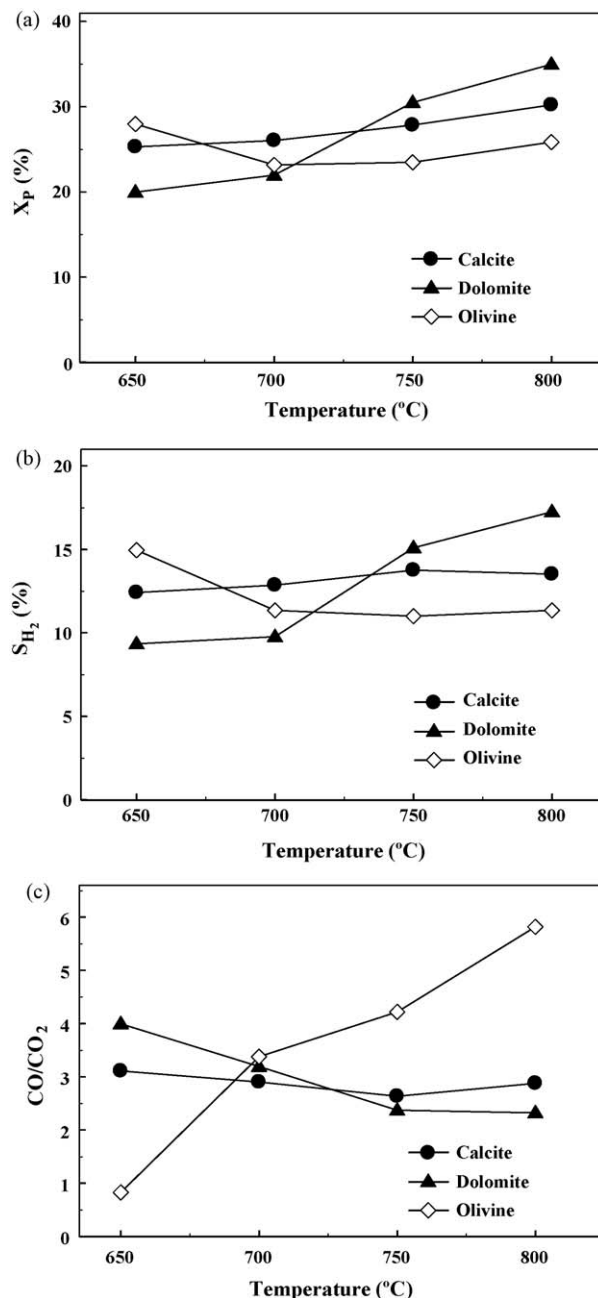


Fig. 7. Dependence of (a) phenol conversion (X_p , %), (b) hydrogen selectivity (S_{H_2} , %), and (c) CO/CO_2 product ratio on the reaction temperature over the naturally occurring calcite, dolomite, and olivine materials. Feed composition: 0.6 vol% $\text{C}_6\text{H}_5\text{OH}/40\%\text{H}_2\text{O}/\text{He}$; $W_{\text{cat}} = 0.3\text{ g}$; $F_T = 200\text{ N mL/min}$.

estimated after 30 min on reaction stream where steady-state was achieved. It is important to report here that a blank catalytic performance experiment of the steam reforming of phenol in the presence of quartz wool alone (used to support the solid catalytic bed in the reactor) showed no measurable activity at 650 °C and a phenol conversion lower than 3% in the 700–800 °C range. Based on the catalytic results of Fig. 7a, the contribution of the homogeneous reaction 0.6% $\text{C}_6\text{H}_5\text{OH}/40\%\text{H}_2\text{O}/59.4\%\text{He}$ in the measured catalytic activity in the 700–800 °C range and at a GHSV of about 54,000 h^{-1} is less than 10%.

As shown in Fig. 7a, olivine is significantly more active (40% increase in X_p) compared to dolomite at 650 °C, while at higher reaction temperatures (750 and 800 °C) the opposite is true. The differences in conversion values of olivine and dolomite become

nearly the same at 700 °C. The activity of both natural calcite and dolomite materials was found to increase with increasing reaction temperature in the 650–800 °C range, while the opposite behaviour was observed for the olivine material. In particular, an increase of X_p by 70% and 20% in the case of dolomite and calcite, respectively, was achieved after increasing the reaction temperature from 650 to 800 °C.

The differences in activity among the three naturally occurring materials mentioned above may be related to their surface texture and elemental bulk and surface compositions. This was also pointed out by Devi et al. [47] in an attempt to explain the behaviour of dolomite and olivine towards steam reforming of naphthalene in the 800–900 °C range. Simell et al. [69] and Borgwardt et al. [70] have also reported that the physical properties including pore and particle size of calcites have an influence on the reactivity of the carbonated rocks. Furthermore, a comparative study of various naturally occurring materials for the catalytic decomposition of tarry constituents in fuel gas revealed that the activity of the carbonate rocks increased with decreasing Ca/Mg ratio [69]. The latter may explain the higher activity in terms of phenol conversion of dolomite material compared to calcite in the 750–800 °C range but not at lower temperatures (Fig. 7a).

The reduction of hematite ($\alpha\text{-Fe}_2\text{O}_3$) and magnetite (Fe_3O_4) present in the case of calcined olivine, as revealed from XRD studies (Fig. 1c), could be responsible for the gradual decreasing activity with increasing reaction temperature. Also, as discussed in Section 3.1.2, the presence of $\text{Fe}_{1-x}\text{Mg}_x\text{O}_y$ and $\text{Ca}_2\text{Fe}_2\text{O}_5$ phases in the calcined olivine cannot be excluded. Thus, reduction of these likely active phases forming FeO (less active phase) could also contribute to the observed decrease in phenol conversion by increasing the reaction temperature from 650 to 750 °C, as also suggested by the H_2 -TPR results (Fig. 5). It is noted here that this reduction process was related to the unstable state of olivine during steam reforming due to the presence of a reducing gas environment ($P_{\text{H}_2\text{O}}/P_{\text{H}_2} > 1$) [69].

In order to support the hypothesis mentioned in the previous paragraph, the following experiments were performed. The olivine sample (as received) was first calcined at 850 °C in 20% O_2 /He for 2 h. The catalyst was then exposed to the reaction mixture at 650 °C for 20 min, and then the reaction temperature was increased to 700 °C and the catalyst was left for another 20 min under the reaction feed stream. The sample was then cooled down again to 650 °C under the reaction mixture and left for 20 min. The phenol conversion estimated at 650 °C when the catalyst was first exposed to the reaction mixture was found to be larger by about 20% compared to the value estimated at 700 °C. The latter result agrees very well with the activity drop shown in Fig. 7a observed between 650 and 700 °C. In the latter case the activity was measured at each reaction temperature on a pre-calcined at 850 °C olivine material. These results strongly support the view that in the presence of H_2 reduction of $\alpha\text{-Fe}_2\text{O}_3$ and Fe_3O_4 seems possible leading to a less active $\text{Fe}^{2+}/\text{Fe}^0$ species. It appears that water is not able to re-oxidize these iron species into Fe^{3+} under the present phenol steam reforming reaction conditions.

Considering the activity results obtained at 650 °C (Fig. 7a), even though the calcined dolomite exhibits 14 times larger BET area (m^2/g) than the calcined olivine (Table 1), the latter solid exhibits about 40% larger activity than dolomite. Therefore, it is rather clear that olivine possesses surface catalytic sites with significantly larger *intrinsic site reactivity* than the dolomite material. It should be noted at this point that BET measurements on the used samples run for at least 8 h on reaction stream and after calcination at 850 °C for 2 h did not reveal changes by more than 10% compared to the fresh sample.

The H_2 -selectivity was found to exhibit a similar behaviour to phenol conversion versus temperature profile for all three natural materials (Fig. 7b). It is noted that hydrogen selectivity values for

all three materials are lower than 20% under the tested experimental conditions (Fig. 7b), suggesting that the concentration of hydrogen produced is about four times smaller than the maximum theoretical H_2 concentration expected (11.76 mol%, dry-basis) [34].

Results on the CO/CO_2 product ratio obtained in the 650–800 °C range for the present naturally occurring materials are presented in Fig. 7c. It is observed that the CO/CO_2 ratio for both calcite and dolomite materials decreases with increasing reaction temperature, while the opposite behaviour was found in the case of olivine. The latter behaviour is rather related to the decreasing number density of active sites present in Fe_2O_3 and Fe_3O_4 with increasing reaction temperature, as previously discussed, which seems to affect also to a greater extent the WGS reaction. In fact, the CO/CO_2 product ratio increases nearly seven times when the reaction temperature increases from 650 to 800 °C.

It should be noted that the CO/CO_2 product ratio is determined by the rates of reactions (1) and (2) and by the thermodynamic equilibrium of the water–gas shift reaction (2). The fact that the dolomite material exhibits the largest hydrogen selectivity (Fig. 7b) and the lowest CO/CO_2 product ratio (Fig. 7c) at 750 and 800 °C supports the view that dolomite promotes to a greater extent the water–gas shift reaction. The latter observation was also seen in the case of olivine at 650 °C. It is instructive to show how close to the equilibrium conditions of the WGS reaction the exit stream of the reactor was. In the case of calcite, at 650 °C, using $y_{\text{H}_2} = 0.0173$, $y_{\text{CO}_2} = 0.0038$, $y_{\text{CO}} = 0.012$ and $y_{\text{H}_2\text{O}} = 0.4$ (y_i = mole fraction of gaseous species), and the theoretical equilibrium constant, $K_{\text{WGS,th}} = 1.88$, it is estimated that the theoretical product $y_{\text{CO}_2} \cdot y_{\text{H}_2}$ equals 90.2×10^{-4} , while the corresponding experimental value is only 0.6×10^{-4} . Similarly, at 800 °C it was found that the theoretical product $y_{\text{CO}_2} \cdot y_{\text{H}_2}$ equals 50×10^{-4} , while the corresponding experimental value is only 0.86×10^{-4} ($K_{\text{WGS,th}} = 0.94$; $y_{\text{H}_2} = 0.0188$; $y_{\text{CO}_2} = 0.0046$; $y_{\text{CO}} = 0.0133$; $y_{\text{H}_2\text{O}} = 0.4$). These results clearly demonstrate that under the experimental conditions examined (Fig. 7), the WGS reaction was far from being at equilibrium.

The beneficial effect of water feed concentration on phenol conversion was concluded after studying the steam reforming of phenol reaction in the 650–800 °C range over the same pre-calcined natural materials using the 0.6% $\text{C}_6\text{H}_5\text{OH}/x\%\text{H}_2\text{O}/\text{He}$ ($x = 40\text{--}50$) feed composition. The activity towards phenol conversion and H_2 -selectivity increased after increasing the water composition in the feed for dolomite and olivine in a similar way as previously reported for the calcite material [33,34].

3.2.2. Effect of feed volume flow rate

The effect of feed volume flow rate on phenol conversion, X_p (%) obtained over the pre-calcined natural calcite, dolomite and olivine materials after 30 min on reaction stream at 750 °C is presented in Fig. 8. The phenol and water feed concentrations were kept constant at 0.6 and 40 vol%, respectively, while the total flow rate used was varied in the 150–300 N mL/min range, which corresponds to a GHSV of 40,000–80,000 h^{-1} . It is clearly seen that the activity in terms of phenol conversion gradually decreases by increasing the GHSV (h^{-1}) for all three naturally occurring materials. In particular, for the calcite and dolomite materials a decrease by about 30% in phenol conversion was obtained, while for olivine the decrease in X_p was slightly higher (~38%). The increase of conversion by decreasing the GHSV (h^{-1}) has also been reported previously [34,71,72].

3.2.3. Effect of hydrogen in the feed stream

Fig. 9a and b present the effect of the presence of 15 vol% hydrogen in the feed stream ($\text{C}_6\text{H}_5\text{OH}/\text{H}_2\text{O}/\text{He}$) on phenol conversion and CO/CO_2 product ratio, respectively, obtained over

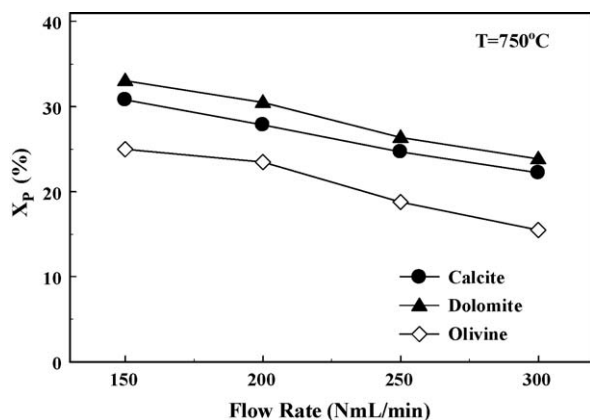


Fig. 8. Dependence of phenol conversion, X_p (%) on total feed volume flow rate for the naturally occurring calcite, dolomite and olivine materials following 30-min of reaction at 750 °C. Feed composition: 0.6 vol% C_6H_5OH /40 vol% H_2O /He; $W_{cat} = 0.3$ g. At the feed volume flow rate of 200 N mL/min the corresponding GHSV is 54,000 h^{-1} .

the natural pre-calcined materials in the 650–800 °C range. The phenol and water feed concentrations were kept constant at 0.6 and 40 vol%, respectively. As shown in Fig. 9a, pre-calcined olivine presented lower conversion values in the 700–800 °C range as compared to the natural calcite and dolomite, while the calcite material presented significantly better activity than dolomite and olivine at all reaction temperatures. A significant decrease in phenol conversion was obtained in the whole temperature range of 650–800 °C after hydrogen feed concentration was increased from 0 to 15 vol% (compare Figs. 7a and 9a). In particular, for the pre-

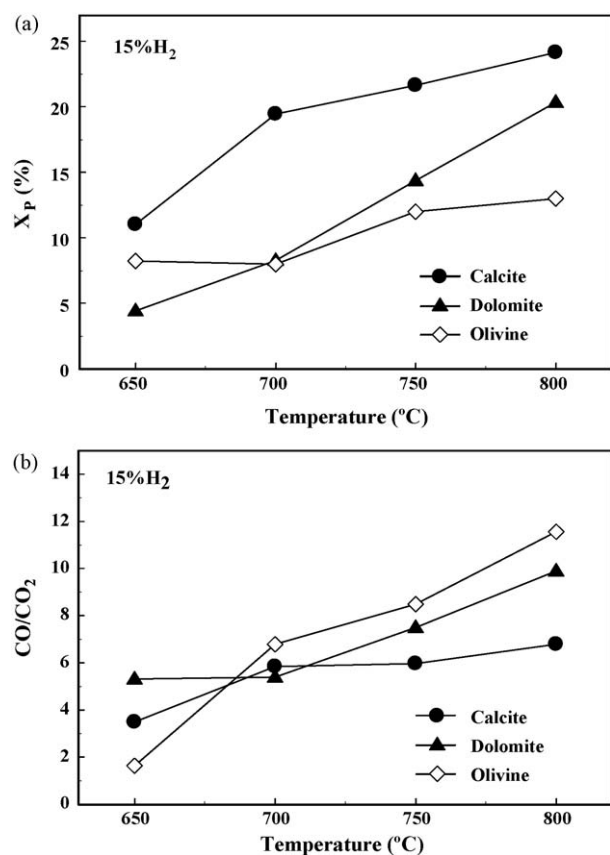


Fig. 9. Dependence of (a) phenol conversion, X_p (%) and (b) CO/CO₂ product ratio on reaction temperature for the naturally occurring calcite, dolomite and olivine materials. Feed composition: 0.6 vol% C_6H_5OH /40 vol% H_2O /15 vol% H_2 /He; $W_{cat} = 0.3$ g; $F_T = 200$ N mL/min.

calcined dolomite and olivine the phenol conversion was decreased by approximately 70% at 650 and 700 °C, while a 50% decrease was observed for the calcite material at 650 °C [34]. A similar behaviour of activity decrease with increasing H_2 concentration in the feed from 0 to 15 vol% H_2 was also obtained in the presence of 30 vol% H_2 in the feed stream. Under the present feed gas compositions used for the phenol steam reforming reaction, it appears that the given calcite material shows the best resistance to activity deterioration in the presence of a strong reducing gas atmosphere (15–30 vol% H_2) compared to dolomite or olivine natural materials. The latter piece of information is very important for biomass gasification applications.

A significant increase in the CO/CO₂ product ratio was also found for all solids tested after the hydrogen feed concentration was increased from 0 to 15 vol% (compare Figs. 7c and 9b). Similar results for the CO/CO₂ product ratio were obtained in the presence of 30 vol% H_2 . This clearly confirms the negative effect of hydrogen feed concentration towards phenol steam reforming activity. According to the results of Fig. 9, the inhibiting effect of hydrogen is substantial for the pre-calcined olivine than the calcite and dolomite materials (700–800 °C), while the opposite behaviour was found at 650 °C. In particular, for olivine an increase by about 50% was found for the CO/CO₂ product ratio after hydrogen feed concentration was increased from 0 to 15 vol% at 800 °C (compare Figs. 7c and 9b).

All the above strongly support the view that the reaction order with respect to H_2 is negative for either the reforming reaction (1) or the water–gas shift reaction (2) or for both reactions. The fact that under the present experimental conditions the WGS reaction is far from being at equilibrium (see Section 3.2.1), any effect of hydrogen on the WGS reaction must relate only to kinetic reasons associated with the forward reaction. As will be shown in the following Section 3.4.1, the effect of hydrogen on catalyst's activity is largely related to the blocking of sites necessary for water dissociation.

It should be mentioned that in the case of olivine the presence of hydrogen clearly contributes to a more severe reduction of α -Fe₂O₃, Fe₃O₄, Fe_{1-x}Mg_xO_y and/or Ca₂Fe₂O₅, which are considered as active phases present in the calcined olivine material (see Section 3.2.1). This justifies the significant decrease of phenol conversion at 800 °C when hydrogen was present in the feed stream. The fact that the decrease in activity is related to the unstable state formed after reduction of Fe^{III}-containing phases present in the calcined olivine has also been reported [48,69].

The strong suppressing effect of hydrogen present in the feed towards steam reforming activity of model compounds of tar is not new [23,26,28]. Extensive studies conducted by several research groups led to the conclusion that hydrogen is dissociatively adsorbed on metal oxide surfaces with the metal cation–oxygen anion pairs being the active sites of adsorption, leading therefore to the blockage of surface active sites [23,26,28,73–76]. Taralas et al. [26] investigated the steam reforming of n-heptane as a model tar compound in the presence of commercial limestone, dolomite, and NiMo/ γ -Al₂O₃ catalysts. They observed that the yield of CO₂ and the total conversion of n-heptane were decreased with the addition of H_2 over calcined dolomite. Aldén et al. [28] and Simell et al. [73] investigated the influence of H_2 on naphthalene and toluene decomposition, respectively over calcined dolomite. They reported that H_2 is a strong inhibitor of the reforming reaction rate due to its dissociative adsorption onto the active sites of calcined dolomite (e.g. Mg^{2+} -O²⁻ and Ca^{2+} -O²⁻). In the following Section 3.4.2, further discussion on this topic is provided.

3.3. Amount of carbonaceous species formed during steam reforming of phenol

The amount (μ mol/g solid) of “carbonaceous” intermediate species formed during phenol steam reforming reaction was

Table 6

Amount ($\mu\text{mol C/g}$) of “carbonaceous” species accumulated on the surface of pre-calcined naturally occurring calcite, dolomite and olivine solids measured by isothermal oxygen titration (20 vol% O_2/He) after 0.6% $\text{C}_6\text{H}_5\text{O}/40\%\text{H}_2\text{O}/\text{He}$ reaction as a function of reaction temperature and time on stream.

Natural material	Temperature ($^{\circ}\text{C}$)	Time on stream (min)	$\mu\text{mol C/g}$
Calcite	650	5	532
		20	583
	800	5	396
		20	555
Dolomite	650	5	227
		20	608
	800	5	183
		20	520
Olivine	650	5	240
		20	460
	800	5	231
		20	442

measured by isothermal oxygen titration (20 vol% O_2/He) following 0.6% $\text{C}_6\text{H}_5\text{OH}/40\%\text{H}_2\text{O}/\text{He}$ reaction at a given temperature and time on stream [34]. The experiments were conducted at 650 and 800 $^{\circ}\text{C}$ for 5 and 20 min of reforming reaction and results are reported in Table 6 for the pre-calcined natural calcite, dolomite and olivine materials. It is seen that the amount of carbonaceous species increases with increasing reaction time, while it varies with reaction temperature depending on the catalyst composition. It is noted that the amount of carbonaceous deposits accumulated after 20 min of reaction might be expected to reach the largest value since the rate of steam reforming reached “steady-state” after about 20 min on stream. This would be true if the accumulated carbonaceous species measured are considered as true reaction intermediates. Moreover, it is noted that the amount of carbonaceous deposits stored on the surface of olivine after 20 min of reforming reaction appears to be lower than that measured in the dolomite and calcite materials. This observation was noticed for both reaction temperatures and it is possibly due to the presence of oxidized Fe (Tables 2 and 4) which is known for its positive effect in lowering the rate of coke formation [49,77]. The latter result may further be the reason for the higher activity measured over the calcined olivine compared to calcite and dolomite at the lowest reaction temperature of 650 $^{\circ}\text{C}$ (Figs. 7a and 9a). However, this is not the case when phenol steam reforming occurred at 800 $^{\circ}\text{C}$, which was previously suggested to be due to the reduction of Fe-containing active phases present in the calcined olivine to less active $\text{Fe}^{\text{II}}\text{O}/\text{Fe}^0$ phases. The presence of higher amounts of MgO in dolomite seems to be a main reason for its better coking resistance compared to calcite observed at 800 $^{\circ}\text{C}$. This could also explain the higher activity of dolomite compared to calcite in the high reaction temperature range of 750–800 $^{\circ}\text{C}$ (Fig. 7a).

3.4. In situ DRIFTS

3.4.1. Chemical structure and thermal stability of adsorbed surface carbonates on dolomite

The different kinds of adsorbed carbonate species formed on the surface of pre-calcined dolomite and their thermal stability were studied using *in situ* DRIFTS under various gas atmospheres. Fig. 10a compares the IR spectra recorded in the 1800–1100 cm^{-1} range (K-M units) after a 2% CO_2/He gas mixture was passed over the pre-calcined dolomite solid sample at room temperature for 30 min followed by an increase of the solid temperature to 100, 300 and 600 $^{\circ}\text{C}$ under Ar flow. The structure of the various adsorbed carbonate species formed and their corresponding vibrational modes are given in Table 7.

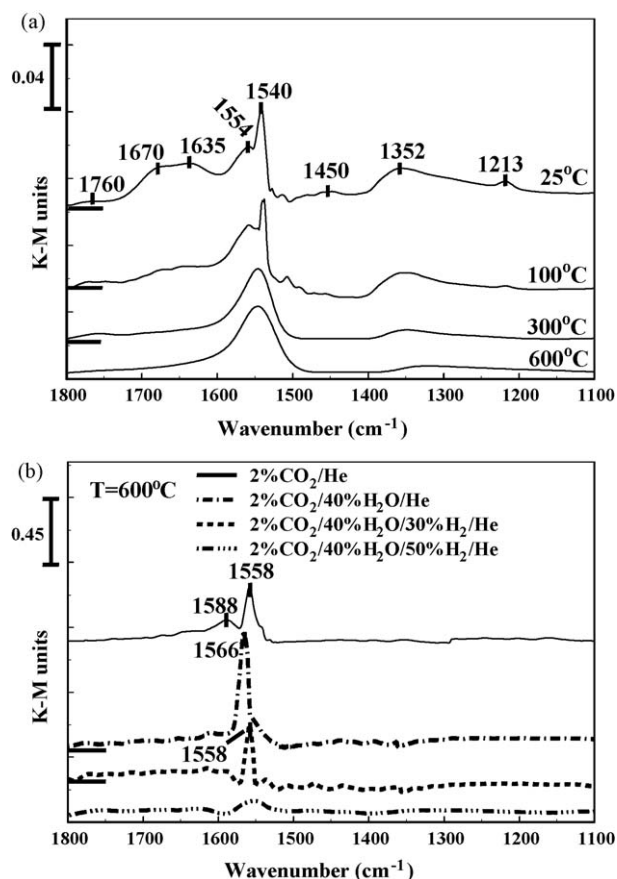


Fig. 10. *In situ* DRIFTS spectra recorded in the 1800–1100 cm^{-1} range after exposing the pre-calcined naturally occurring dolomite in (a) 2 vol% CO_2/He for 30 min at 25 $^{\circ}\text{C}$, and subsequently increasing the solid temperature under Ar flow to 100, 300 and 600 $^{\circ}\text{C}$, and (b) 2 vol% CO_2/He or 2 vol% $\text{CO}_2/40\%\text{H}_2\text{O}/\text{He}$ or 2 vol% $\text{CO}_2/40\%\text{H}_2\text{O}/30\%\text{H}_2/\text{He}$ or 2 vol% $\text{CO}_2/40\%\text{H}_2\text{O}/50\%\text{H}_2/\text{He}$ gas mixture at 600 $^{\circ}\text{C}$ for 30 min.


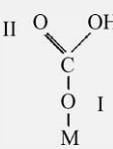
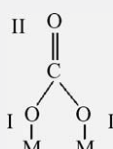
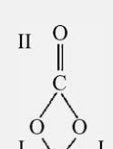
In the case of CO_2 chemisorption at room temperature, the weak IR band recorded at 1760 cm^{-1} is attributed to the C–O stretching vibrational mode of bridging carbonate [78–81], while the shoulder bands centred at 1670 and 1635 cm^{-1} are assigned to the OCO_{as} vibrational mode of two different bicarbonate species (e.g. different site location). In addition, the IR bands at 1554 and 1540 cm^{-1} are due to the asymmetric OCO_{as} stretching mode of unidentate carbonate, while the IR band at 1352 cm^{-1} to the symmetric OCO_{s} vibrational mode of unidentate carbonate [80–84]. The weaker and broad IR bands centred at 1450 and 1213 cm^{-1} are assigned to the OCO_{s} stretching and COH bending vibrational modes, respectively, of bicarbonate species [78,80–83].

According to the DRIFTS results presented above, unidentate carbonate seems to be the dominant adsorption state of carbon dioxide at 25 $^{\circ}\text{C}$, while bicarbonate is formed in lower concentrations and bridging carbonate in minor concentrations. These results support the view that dolomite behaves like a CaO-rich material (MgO content < 50 wt%) [80,81] in agreement with its elemental composition (Table 2).

After increasing the temperature of the solid to 100 $^{\circ}\text{C}$ under Ar flow (Fig. 10a), a decrease in the surface concentration of all carbonates formed is observed, where bicarbonate species (1670, 1635 cm^{-1}) appear to be the least thermally stable. This indicates the onset of bicarbonate decomposition which is known to have a lower thermal stability than unidentate carbonate [81]. The surface concentration of bicarbonate species becomes practically zero after increasing the temperature to 300 $^{\circ}\text{C}$. The disappearance

Table 7

Chemical structures of adsorbed species formed upon CO₂ interaction with pre-calcined naturally occurring calcite, dolomite and olivine and their corresponding IR vibrational modes.

Carbonate structure	Wavenumber (cm ⁻¹)	Assignment	Ref.
	1540–1580 1350–1390	O _i CO ₃ as O _i CO ₃ s	[80–84]
	1630–1680 1410–1480 1213–1226	O _i CO ₃ as O _i CO ₃ s COH bending	[78–83]
	1770–1780	CO ₃ stretching	[78–81]
	1560–1629	O _i CO ₃ as	[78,81,85]

M: Ca, Mg, Fe.

of the shoulder band at 1554 cm⁻¹, which corresponds to unidentate carbonate, was also observed. It is noted that the thermal decomposition of the latter species formed on the surface of pre-calcined calcite started at 600 °C [34]. These results are in full agreement with the fact that the desorption temperature of unidentate carbonate increases with increasing CaO content [81].

When dolomite was heated to 600 °C in Ar flow (Fig. 10a), the small IR band centered at 1760 cm⁻¹ completely disappeared, while the IR bands recorded in the 1500–1100 cm⁻¹ range were absent or largely reduced. The band at 1540 cm⁻¹ corresponding to unidentate carbonate was less affected. The shoulder to the higher wavelength-side of the band at 1540 cm⁻¹ may suggest the presence of bidentate carbonate [86]. The fact that the surface coverage of the unidentate carbonate did not reach the zero value even when the temperature was increased to 600 °C confirms the high thermal stability of this species.

Fig. 10b compares the DRIFTS spectra recorded in the 1800–1100 cm⁻¹ range (K–M units) after a 30-min exposure of the calcined dolomite to various gas atmospheres at 600 °C, namely: 2%CO₂/He, 2%CO₂/40%H₂O/He and 2%CO₂/40%H₂O/30 or 50%H₂/He. In particular, after 30-min treatment of the pre-calcined dolomite with a 2%CO₂/He at 600 °C a small IR band centred at 1588 cm⁻¹ and a sharp larger IR band at 1558 cm⁻¹ were observed, and these are assigned to bidentate and unidentate carbonates, respectively [34,80,81,84,85]. It should be noted that the surface concentration of all carbonates formed is larger compared to that obtained following CO₂ chemisorption at room temperature (Fig. 10a), in agreement with previously reported observations [78]. After exposure of the pre-calcined dolomite to 2%CO₂/40%H₂O/He for 30 min at 600 °C, the IR band corresponding to unidentate carbonate was significantly increased and shifted slightly to higher wavenumbers (1566 cm⁻¹) compared to that

obtained following CO₂/He treatment (Fig. 10b). The shoulder band detected in the higher wavelength-side may possibly suggest the co-existence of bicarbonate, bidentate or formate species [34,84].

In the case of CO₂ chemisorption in the presence of 40 vol% of H₂O and 30 vol% of H₂, the IR band corresponding to unidentate carbonate (1558 cm⁻¹) was decreased, while the broad IR band recorded in the 1800–1570 cm⁻¹ range was slightly increased compared to that recorded in the absence of hydrogen in the gas treatment atmosphere. The broad band observed in the 1800–1570 cm⁻¹ range is consistent to the presence of bicarbonate (1680–1620 cm⁻¹) and formate (1610 cm⁻¹) species, the latter also formed after CO₂/H₂ adsorption [84]. After increasing the H₂ feed concentration to 50 vol% in the H₂/CO₂/H₂O/He gas mixture, the surface concentrations of bicarbonate, formate and unidentate species were reduced (Fig. 10b).

3.4.2. Probing the negative effect of H₂ on the activity of dolomite

Fig. 11a compares the IR spectra (absorbance mode) recorded in the 3700–3300 cm⁻¹ range after a 40%H₂O/30%H₂/Ar gas mixture was passed at 600 °C for 30 min over the pre-calcined (850 °C) dolomite material with a subsequent isothermal purge in Ar gas-flow for 30 min. The large broadening of the ν-OH region observed in Fig. 11a is due to the distribution of various possible kinds of –OH species formed on the surface of a metal oxide and the presence of Mg(OH)₂ and Ca(OH)₂ formed upon treatment of initial MgO/CaO (calcined dolomite) with water [87–89]. The development of the –OH integral band area observed under the 40%H₂O/30%H₂/Ar gas treatment is shown in Fig. 11b for 2, 10 and 30 min on stream. The variation of this integral band area after 30 min in Ar purge (Fig. 11a) is also shown in Fig. 11b. It is clearly observed that the concentration of –OH species formed on the MgO and CaO surfaces increases in the first 10 min of treatment, while only a small increase is observed for longer times on stream. On the other hand, a significant decrease in the concentration of –OH species is observed upon isothermal Ar purge of the catalyst sample. The latter is due to a de-hydroxylation process taking place on the MgO/Mg(OH)₂ and CaO/Ca(OH)₂ surface/subsurface at 600 °C in accordance also to the literature [88,89].

When adsorption of 40 vol% H₂O took place for 30 min from a gas mixture containing 30 or 50 vol% of H₂, a significant reduction in the concentration of hydroxyl species formed on the initial MgO and CaO surfaces was observed as depicted in Fig. 11c. Given the description of results of the blank DRIFTS experiments performed under 30 or 50%H₂/Ar gas mixtures (see Section 2.4), it is clear that the presence of H₂ in the H₂/40%H₂O/Ar gas mixture causes a significant decrease in the concentration of –OH species formed.

Martino et al. [90] described in a very elegant way the H₂ chemisorption behaviour on the MgO surface. At room temperature an irreversible chemisorption saturated at <0.1 mbar H₂ pressure is associated with the formation of stable hydride species (HMg–OH) associated with a very low concentration of 3-coordinated Mg²⁺ cations. In contrast, the sites responsible for the more abundant reversible dissociation (splitting) of the H₂ molecule are far less known. On the other hand, the fact that the H₂ molecule is reversibly adsorbed on the surface should imply that the H⁺ and H⁻ fragments are still experiencing a substantial degree of electrostatic interaction in the chemisorbed state [90]; a positive region stabilizes the H⁻ fragment and a negative region stabilizes the H⁺ fragment. A similar phenomenon to that reported in Fig. 11c was observed in chemisorption studies on the MgO surface using different mixtures of NO/H₂ [90]. For low hydrogen pressures (H₂:NO = 1:10) surface coverage of NO was maximum, while for high hydrogen pressures (H₂:NO = 1:1) the surface coverage of NO vanished.

Based on the above-offered discussion, it is rather clear that in the present case the significant decrease in the concentration of –OH groups upon increasing the H₂ pressure from 0.3 to 0.5 bar

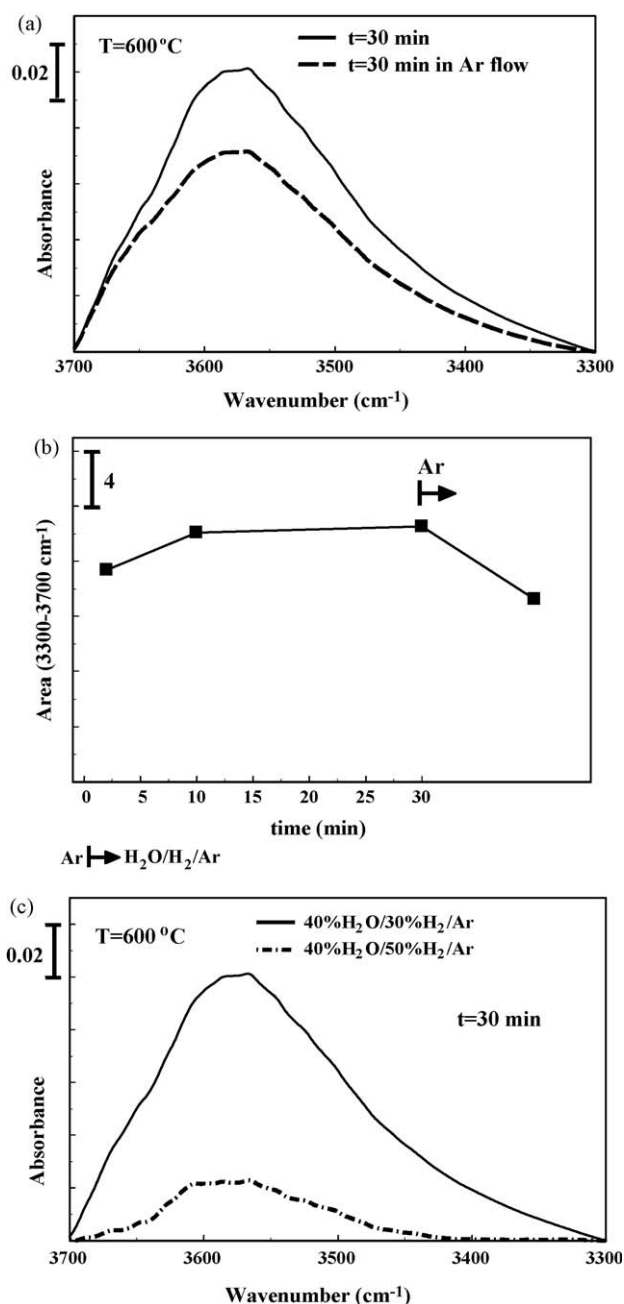


Fig. 11. (a) *In situ* DRIFTS spectra recorded in the 3700–3300 cm⁻¹ range after exposing the pre-calcined naturally occurring dolomite in 40% H₂O/30% H₂/Ar gas mixture for 30 min at 600 °C and after a 30-min isothermal purge in Ar flow. (b) Integral band area of the –OH species formed following a 40% H₂O/30% H₂/Ar treatment of the dolomite solid for 2, 10 and 30 min followed by a 30-min Ar purged at 600 °C. (c) *In situ* DRIFTS spectra recorded in the 3700–3300 cm⁻¹ range after exposing the pre-calcined dolomite in a 40 vol% H₂O/30 vol% H₂/He or 40 vol% H₂O/50 vol% H₂/He gas mixture at 600 °C for 30 min.

cannot be due to an irreversible competitive adsorption between H₂ and H₂O molecules. It is suggested that this is rather due to an inhibiting effect imposed by the reversible kind of H₂ interaction with the MgO/CaO surface on the water chemisorption. The nature of this inhibiting hydrogen effect is not known, but it seems to be related to a reducing electrostatic interaction between the surface and the water molecules imposed by the presence of hydrogen molecules in such a high concentration. Irrespective of the exact mechanism of hydrogen inhibiting effect on water chemisorption and dissociation to form –OH species, this observable effect is well correlated with the activity results reported in Section 3.2.1, where

a significant reduction in dolomite's activity was seen when 15 or 30 vol% H₂ was present in the feed stream. The present DRIFTS results (Fig. 11) strongly suggest that –OH species are important reaction intermediates for the conversion of phenol into CO_x and H₂ gas products.

It is noted that dolomite resulted in lower values of phenol conversion compared to calcite material at 650 °C. This could be related to the higher surface coverage of carbonate species formed (Fig. 10b) compared to the pre-calcined calcite material reported previously [34], where carbonates compete for the same sites as phenol and water reactant molecules.

3.4.3. Chemical structure and thermal stability of adsorbed surface carbonates on olivine

The *in situ* DRIFTS studies described in Section 3.4.1 were also performed over the pre-calcined natural olivine material. Fig. 12a compares the *in situ* DRIFTS spectra recorded in the 1800–1100 cm⁻¹ range (K–M units) after exposure of the pre-calcined olivine to a 2% CO₂/He gas mixture at room temperature for 30 min followed by an increase of the solid temperature to 100, 300 and 600 °C under Ar flow. The most intense IR bands were detected at 1633, 1538, 1516, 1414 and 1386 cm⁻¹ (Fig. 12a) and are attributed to bicarbonate and unidentate carbonate species. More precisely, the broad IR bands at 1633 and 1414 cm⁻¹ correspond to OCO_{as} and OCO_s vibrational modes, respectively of bicarbonate species, while the IR bands centered at 1538, 1516 and 1386 cm⁻¹ to the OCO_{as} vibrational mode of two different kinds of unidentate carbonates, and to the symmetric OCO_s vibrational mode of

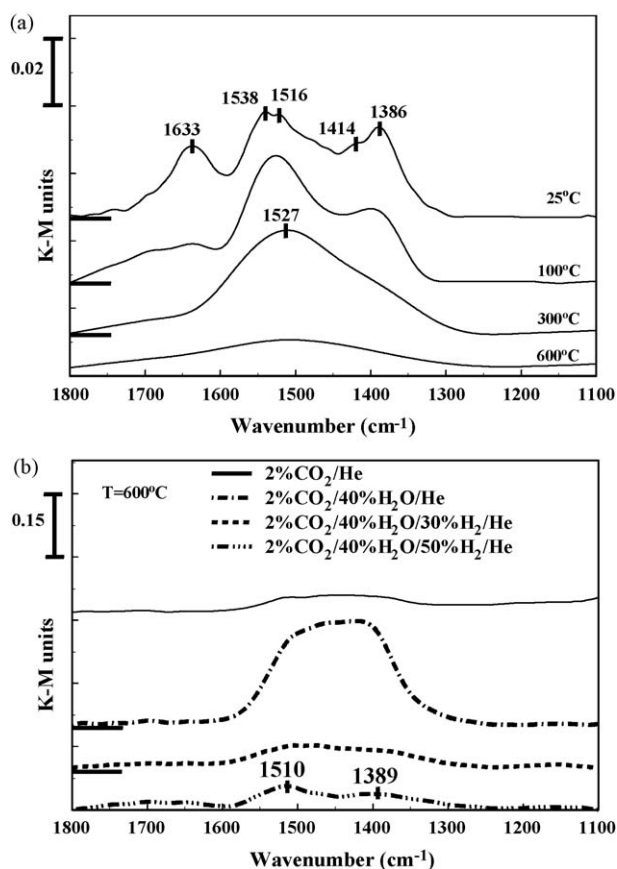


Fig. 12. *In situ* DRIFTS spectra recorded in the 1800–1100 cm⁻¹ range after exposing the pre-calcined natural olivine material in (a) 2 vol% CO₂/He gas mixture at 25 °C for 30 min and subsequently increasing the solid temperature under Ar flow to 100, 300, and 600 °C; (b) 2 vol% CO₂/He or 2 vol% CO₂/40 vol% H₂O/He or 2 vol% CO₂/40 vol% H₂O/30 vol% H₂/He or 2 vol% CO₂/40 vol% H₂O/50 vol% H₂/He gas mixture at 600 °C for 30 min.

unidentate carbonate, respectively [80–84,86]. The intensities of all infrared bands were decreased after the solid was heated in Ar flow to 100 °C. This decrease was large for the 1633 cm⁻¹ IR band (bicarbonate) leading to the conclusion that this species is thermally unstable. The IR bands corresponding to unidentate carbonate remained practically unchanged. When the catalyst was heated to 300 °C the IR bands corresponding to bicarbonates disappeared except those of unidentate. For the latter species a single IR band centred at 1527 cm⁻¹ was seen (Fig. 12a). After the temperature was increased to 600 °C the surface coverage of unidentate carbonate (1527 cm⁻¹) was drastically reduced. The DRIFTS-TPD run shown in Fig. 12a illustrates that the decomposition of the various carbonate structures formed after CO₂ chemisorption on the surface of pre-calcined olivine is almost completed at 600 °C in accordance with the TPD-Mass spectrometry studies (Fig. 6).

Fig. 12b compares the DRIFTS spectra recorded in the 1800–1100 cm⁻¹ range (K–M units) after a 30-min exposure of the pre-calcined olivine with various CO₂-containing gas atmospheres at 600 °C. It is observed that the surface concentration of carbonates when CO₂/He was passed over the olivine at 600 °C (Fig. 12b) was significantly lower than that obtained after chemisorption of CO₂ at room temperature (Fig. 12a), in agreement with the results reported in Fig. 6, where desorption of CO₂ was completed up to 600 °C. This leads to the conclusion that the surface basic sites of olivine are weaker compared to those present in calcite and dolomite materials. When CO₂ adsorption was contacted in the presence of 40 vol% H₂O, the intensities of the IR bands recorded in the 1600–1300 cm⁻¹ range were significantly increased. The large broad band observed suggests the possible co-existence of bicarbonates (1680–1620 and 1480–1410 cm⁻¹) [80–84], unidentate (1580–1560 and 1390–1360 cm⁻¹) [80,81], formate (OCO_{as}, 1600 cm⁻¹) [84], and/or bidentate carbonate (1580 and 1300 cm⁻¹) species [79–81]. These results are in agreement with those previously reported after conducting similar *in situ* DRIFTS studies over the pre-calcined calcite material [34,91].

CO₂ chemisorption in the presence of 40 vol% H₂O and 30 vol% H₂ resulted in a significant decrease in the intensity of the broad IR band observed in the 1600–1300 cm⁻¹ range. The presence of 30 vol% H₂ led to the formation of more discerned IR bands at 1510 and 1389 cm⁻¹ which correspond to the OCO_{as} and OCO_s stretching modes of unidentate carbonate. After increasing the H₂ concentration to 50 vol% (Fig. 12b) in the H₂/CO₂/H₂O gas mixture, the surface concentration of unidentate carbonate (1510 and 1389 cm⁻¹) remained practically the same. A similar decrease in the surface concentration of –OH groups (e.g. 3543 cm⁻¹) as that shown in Fig. 11c was also observed (not reported here) when adsorption of CO₂ took place from a gas mixture containing 40 vol% H₂O and H₂ in the 30–50 vol% range.

4. Conclusions

The following conclusions can be derived from the results of the present work:

- The increase of reaction temperature in the 650–800 °C range results in an increase of phenol steam reforming activity and selectivity towards H₂ over both dolomite and calcite materials. The opposite was observed in the case of olivine. In the case of dolomite, a 75% increase was obtained by increasing the reaction temperature from 650 to 800 °C.
- It was found that phenol conversion increases with decreasing GHSV in the 40,000–80,000 h⁻¹ range at 750 °C for all three naturally occurring materials studied.
- The activity of natural calcite, dolomite and olivine materials per gram basis towards steam reforming of phenol is not correlated

with their BET surface area (m²/g) but rather to the *different intrinsic surface site reactivity* exhibited by the individual solid phases present, which is influenced by the surface morphology and chemical composition of the primary crystals.

- X-ray diffraction and X-ray photoelectron spectroscopy studies revealed the presence of FeO (wüstite) structure in the raw olivine natural material. After calcination in air at 850 °C the formation of α-Fe₂O₃ (hematite) and Fe₃O₄ (magnetite) structures were detected without excluding the presence of Fe_xMg_{1-x}O_y and Ca₂Fe₂O₅ phases.
- The significantly lower activity (per gram basis) at high temperatures (750–800 °C) of pre-calcined olivine compared to pre-calcined calcite and dolomite materials is suggested to be linked to the reducibility of α-Fe₂O₃ and Fe₃O₄ structures, and of Fe_xMg_{1-x}O_y and Ca₂Fe₂O₅ phases likely present in the pre-calcined olivine into less active Fe^{II}O and Fe⁰.
- The higher activity of calcined olivine compared to calcite and dolomite materials at the lower reaction temperature of 650 °C is suggested to be linked to the higher site reactivity and lower concentration of “carbon” accumulated on its surface after steam reforming of phenol, as well as to the lower surface concentration of various kinds of inactive carbonates and formate species formed (*in situ* DRIFTS studies conducted at 600 °C in the presence of CO₂/H₂O/H₂ gas mixtures).
- The effect of H₂ concentration in the feed stream (15–30 vol%) on the phenol steam reforming activity appears to be strongly negative for all three naturally occurring materials investigated, leading also to a significant increase in the CO/CO₂ product ratio. The best material with the largest resistance to activity deterioration appears to be the calcite under the examined catalytic reaction conditions.
- In situ* DRIFTS-CO₂ chemisorption studies showed that the surface coverage of all carbonate-like adsorbed species formed on the pre-calcined surface of calcite and dolomite increase with increasing chemisorption temperature (25–600 °C). The opposite behaviour was observed for the pre-calcined olivine material. These results are in agreement with those obtained in CO₂-TPD studies.
- A significant decrease in the surface concentration of –OH groups was observed when a 40 vol% H₂O and H₂ in the 15–50 vol% range (40% H₂O/x% H₂/He) passed over all three naturally occurring materials investigated. The latter result parallels the strong inhibiting effect of H₂ observed on the phenol steam reforming reaction rate, when hydrogen is co-fed in the phenol/water reaction gas mixture, thus suggesting the important role of –OH species in the mechanism of phenol steam reforming.

Acknowledgements

The financial support of the European Union through the project No. 5183309 (SES6), 6th FP, and of the Research Committee of the University of Cyprus is gratefully acknowledged.

References

- L. Devi, K.J. Ptasiński, F.J.J.G. Janssen, *Biomass Bioenergy* 24 (2003) 125.
- J.N. Armor, *Appl. Catal. A: Gen.* 176 (1999) 159.
- R.C. Saxena, D. Seal, S. Kumar, H.B. Goyal, *Renew. Sustain. Energy Rev.* 12 (2008) 1909.
- C. Koroneos, A. Dompas, G. Roumbas, *Chem. Eng. Proc.* 47 (2008) 1261.
- G. Marbán, T. Valdés-Solís, *Int. J. Chem. Rec. Eng.* 32 (2007) 1625.
- R.R. Davda, J.W. Shabaker, G.H. Huber, R.D. Cortright, J.A. Dumesic, *Appl. Catal. B: Environ.* 56 (2005) 171.
- S. Yaman, *Energy Convers. Manage.* 45 (2004) 651.
- M. Ni, D.Y.C. Leung, M.K.H. Leung, K. Sumathy, *Fuel Proc. Technol.* 87 (2006) 461.
- D. Dayton, A Review of the Literature on the Catalytic Biomass Tar Destruction, NREL/TP-510-32815, National Renewable Energy Laboratory, 2002.
- C. Franco, F. Pinto, I. Gulyurtlu, I. Gabrita, *Fuel* 82 (2003) 835.

- [11] S. Rapagnà, N. Jand, P.U. Foscolo, *Int. J. Hydrogen Energy* 23 (1998) 551.
- [12] L. Shen, Y. Gao, J. Xiao, *Biomass Bioenergy* 32 (2) (2008) 120.
- [13] T.A. Milne, N. Abatzoglou, R.J. Evans, *Biomass Gasifier Tars: Their Nature, Formation and Conversion*, NREL/TP-570-25357, National Renewable Energy Laboratory, USA, 1989.
- [14] R. Zhang, R.C. Brown, A. Suby, K. Cummer, *Energy Convers. Manage.* 45 (2004) 995.
- [15] L. Garcia, M.L. Salvador, J. Arauzo, R. Bilbao, *Energy Fuels* 13 (1999) 851.
- [16] C. Brage, Q. Yu, K. Sjöström, *Fuel* 75 (2) (1996) 213.
- [17] European Project, 6th FP, No. 5183309 (SES6), *Biomass Fluidized Bed Gasification with In-Situ Hot Gas Cleaning*, 2006–2009.
- [18] J. Corella, M.-P. Aznar, J. Gil, M.A. Caballero, *Energy Fuels* 13 (1999) 1122.
- [19] D. Sutton, B. Kelleher, J.R.H. Ross, *Fuel Proc. Technol.* 73 (2001) 155.
- [20] J. Delgado, M.-P. Aznar, J. Corella, *Ind. Eng. Chem. Res.* 35 (1996) 3637.
- [21] A. Olivares, M.-P. Aznar, M.A. Caballero, J. Gil, E. Francés, J. Corella, *Int. J. Hydrogen Energy* 36 (1997) 5220.
- [22] A. Orio, J. Corella, I. Narvaez, *Int. J. Hydrogen Energy* 36 (1997) 3800.
- [23] P.A. Simell, E.K. Hirvensalo, V. Smolander, A.O.I. Krause, *Ind. Eng. Chem. Res.* 38 (1999) 1250.
- [24] P.A. Simell, J.K. Leppälähti, E.A. Kurkela, *Fuel* 74 (6) (1995) 945.
- [25] G. Taralas, V. Vassiliatos, K. Sjöström, J. Delgado, *Can. J. Chem. Eng.* 69 (6) (1991) 1413.
- [26] G. Taralas, *Ind. Eng. Chem. Res.* 35 (1996) 2121.
- [27] P. Pérez, P.-M. Aznar, M.A. Caballero, J.A. Martín, J. Corella, *Energy Fuels* 11 (1997) 1194.
- [28] H. Aldén, E. Björkman, M. Carlsson, A. Waldheim, in: *Proceedings of Conference on Advances in Thermochemical Biomass Conversion*, Blackie Academic & Professional, London, 1994, p. 216.
- [29] S. Rapagnà, N. Jand, A. Kiennemann, P.U. Foscolo, *Biomass Bioenergy* 19 (2000) 187.
- [30] J. Corella, J.-M. Toledo, R. Padilla, *Energy Fuels* 18 (2004) 713.
- [31] J. Delgado, M.-P. Aznar, J. Corella, *Ind. Eng. Chem. Res.* 36 (1997) 1535.
- [32] X. Garcia, N.A. Alarcon, A.L. Gordon, *Fuel Proc. Technol.* 58 (1999) 83.
- [33] D.A. Constantinou, A.M. Efstathiou, *Catal. Today* 143 (2009) 17.
- [34] D.A. Constantinou, J.L.G. Fierro, A.M. Efstathiou, *Appl. Catal. B: Environ.* 90 (2009) 347.
- [35] A.L. Patterson, *Phys. Rev.* 56 (1939) 978.
- [36] C.D. Warner, L.E. Davis, M.V. Zeller, J.A. Taylor, R.H. Raymond, L.H. Gale, *Surf. Interface Anal.* 3 (1981) 211.
- [37] C.N. Costa, T. Anastasiadou, A.M. Efstathiou, *J. Catal.* 194 (2000) 250.
- [38] K. Polychronopoulou, C.N. Costa, A.M. Efstathiou, *Appl. Catal. A: Gen.* 272 (2004) 37.
- [39] K. Polychronopoulou, J.L.G. Fierro, A.M. Efstathiou, *J. Catal.* 228 (2004) 417.
- [40] K. Polychronopoulou, A. Bakandritsos, V. Tzitzios, J.L.G. Fierro, A.M. Efstathiou, *J. Catal.* 241 (2006) 132.
- [41] M.R. Mahishi, D.Y. Goswami, *Int. J. Hydrogen Energy* 32 (2007) 2803.
- [42] B. Balasubramanian, A.L. Ortiz, S. Kaytakoglu, D.P. Harrison, *Chem. Eng. Sci.* 54 (1999) 3543.
- [43] B.C. Smith, *Fundamentals of Fourier Transform Infrared Spectroscopy*, CRC Press, 1996.
- [44] F.M. Hoffmann, *Surf. Sci. Rep.* 3 (1983) 107.
- [45] H. Gupta, L.-S. Fan, *Ind. Eng. Chem. Res.* 41 (2002) 4035.
- [46] K. Chrissafis, C. Dagounaki, K.M. Paraskevopoulos, *Thermochim. Acta* 428 (2005) 193.
- [47] L. Devi, K.J. Ptasiński, F.J.J.G. Janssen, S.V.B. van Paasen, P.C.A. Bergman, J.H.A. Kiel, *Renew. Energy* 30 (2005) 565.
- [48] L. Devi, M. Craje, P. Thüne, K.J. Ptasiński, F.J.J.G. Janssen, *Appl. Catal. A: Gen.* 294 (2005) 68.
- [49] G. Hu, S. Xu, S. Li, C. Xiao, S. Liu, *Fuel Proc. Technol.* 87 (2006) 375.
- [50] N. Saikia, G. Cornelis, G. Mertens, J. Elsen, K. Van Balen, T. Van Gerven, C. Vandecasteele, *J. Hazard. Mater.* 154 (2008) 766.
- [51] C. Courson, L. Udrón, D. Świerczyński, C. Petit, A. Kiennemann, *Catal. Today* 76 (2002) 75.
- [52] J.N. Kuhn, Z. Zhao, L.G. Felix, R.B. Slimane, Chum.W. Choi, U.S. Ozkan, *Appl. Catal. B: Environ.* 81 (2008) 14.
- [53] Y. Hou, Z. Xu, S. Sun, *Angew. Chem. Int. Ed.* 46 (2007) 6329.
- [54] W.K. Jozwiak, E. Kaczmarek, T.P. Maniecki, W. Ignaczak, W. Maniukiewicz, *Appl. Catal. A: Gen.* 326 (2007) 17.
- [55] D.K. Mukhopadhyay, D.H. Lindsley, *Am. Miner.* 68 (1983) 1089.
- [56] Y.S. Liu, J.L. Chen, C.L. Chen, C.L. Dong, D.S. Lee, G. Chern, C.L. Chang, *J. Alloys Compd.* 442 (2007) 259.
- [57] N. Sharma, K.M. Shaju, G.V. Subba Rao, B.V.R. Chowdari, *Electrochim. Acta* 49 (2004) 1035.
- [58] D. Hirabayashi, T. Yoshikawa, K. Mochizuki, K. Suzuki, Y. Sakai, *Catal. Lett.* 110 (2006) 269.
- [59] P. Fenter, Z. Zhang, C. Park, N.C. Sturchio, X.M. Hu, S.R. Higgins, *Geochim. Cosmochim. Acta* 71 (2007) 566.
- [60] D.R. Baer, J.F. Moulder, *Surf. Sci. Spectra* 2 (1993) 1.
- [61] D.R. Baer, A.M. Marmorstein, R.E. Williford, D.L. Blanchard, *Surf. Sci. Spectra* 1 (1993) 80.
- [62] S.L. Stipp, M.F. Hochella Jr., G.A. Parks, J.O. Leckie, *Cheochim. Cosmochim. Acta* 56 (1992) 1941.
- [63] X. Hu, P. Joshi, S.M. Mukhopadhyay, S.R. Higgins, *Cheochim. Cosmochim. Acta* 56 (2006) 3342.
- [64] P. Mills, J.L. Sullivan, *J. Phys. D: Appl. Phys.* 16 (1983) 723.
- [65] C.R. Brundle, T.J. Chuang, K. Wandelt, *Surf. Sci.* 68 (1997) 459.
- [66] G. Zhang, H. Hattori, K. Tanabe, *Appl. Catal.* 36 (1988) 189.
- [67] K. Omata, A. Aoki, K. Fujimoto, *Catal. Lett.* 4 (1990) 241.
- [68] J.-A. Wang, L.-F. Chen, C.-L. Li, *React. Kinet. Catal. Lett.* 64 (1) (1998) 73.
- [69] P.A. Simell, J.K. Leppälähti, J.B.-S. Bredenberg, *Fuel* 71 (1992) 211.
- [70] R.H. Borgwardt, R.D. Harvey, *Environ. Sci. Technol.* 6 (1972) 350.
- [71] D. Wang, S. Czernik, D. Montané, M. Mann, E. Chornet, *Ind. Eng. Chem. Res.* 36 (1997) 1507.
- [72] S. Adhikari, S. Fernando, A. Haryanto, *Catal. Today* 129 (2007) 355.
- [73] P.A. Simell, J.O. Hepola, A.O.I. Krause, *Fuel* 76 (12) (1997) 1117.
- [74] H. Kobayashi, M. Yamaguchi, T. Ito, *J. Phys. Chem.* 94 (1990) 7206.
- [75] H. Kobayashi, D.R. Salahub, T. Ito, *J. Phys. Chem.* 98 (1994) 5487.
- [76] H. Hattori, *Chem. Rev.* 95 (1995) 537.
- [77] A.V. Kucherova, V.D. Nissenbaum, T.N. Kucherova, L.M. Kustov, *Kinet. Catal.* 43 (2002) 711.
- [78] Y. Xu, L. Yu, C. Cai, J. Huang, X. Guo, *Catal. Lett.* 35 (1995) 215.
- [79] N. Alarcón, X. Garcia, M. Centeno, P. Ruiz, A. Gordon, *Surf. Interface Anal.* 31 (2001) 1031.
- [80] R. Philipp, K. Fujimoto, *J. Phys. Chem.* 96 (1992) 9035.
- [81] R. Philipp, K. Omata, A. Aoki, K. Fujimoto, *J. Catal.* 134 (1992) 422.
- [82] M.I. Zaki, H. Knözinger, B. Tesche, G.A.H. Mekhemer, *J. Colloid Interface Sci.* 303 (2006) 9.
- [83] M.I. Zaki, H. Knözinger, B. Tesche, G.A.H. Mekhemer, H.-J. Bongard, *Langmuir* 24 (2008) 6745.
- [84] G. Busca, V. Lorenzelli, *Mater. Chem.* 7 (1982) 89.
- [85] Y. Fukuda, K. Tanabe, *Bull. Chem. Soc. Jpn.* 46 (1973) 1616.
- [86] A.A. Davydov, M.L. Shepotko, A.A. Budneva, *Catal. Today* 24 (1995) 225.
- [87] C. Chizallet, G. Costentin, M. Che, F. Delbecq, P. Sautet, *J. Am. Chem. Soc.* 129 (20) (2007) 6442.
- [88] R.L. Frost, J.T. Klopogge, *Spectrochim. Acta A* 55 (1999) 2195.
- [89] N. Takezawa, *Bull. Chem. Soc. Jpn.* 44 (1971) 3177.
- [90] P. Martino, M. Chiesa, M.C. Paganini, E. Giamello, *Surf. Sci.* 527 (2003) 80, and references therein.
- [91] A.A. Medvinskii, G.G. Saveliev, N.F. Stas', O.V. Tyunina, V.V. Nakhalov, I.A. Kononova, P.D. Khalfma, *React. Kinet. Catal. Lett.* 6 (2) (1977) 139.